Ecotoxicology and Environmental Safety 226 (2021) 112838

Contents lists available at ScienceDirect

Ecotoxicology and Environmental Safety

journal homepage: www.elsevier.com/locate/ecoenv

New insights into benzo[α]pyrene osteotoxicity in zebrafish

Marco Tarasco [a], Paulo J. Gavaia [a,b], Anabela Bensimon-Brito [c,d,e], João Cardeira-da-Silva [c], Srinath Ramkumar [c,f], Fabrice P. Cordelières [h], Stefan Günther [d,g], Maria J. Bebianno [i], Didier Y. R. Stainier [c], M. Leonor Cancela [a,b], Vincent Laizé [a,*]

[a] Centre of Marine Sciences (CCMAR), University of Algarve, Faro, Portugal
[b] Faculty of Medicine and Biomedical Sciences (FMCB) and Algarve Biomedical Center (ABC), University of Algarve, Faro, Portugal
[c] Max Planck Institute for Heart and Lung Research, Department of Developmental Genetics, Bad Nauheim, Germany
[d] DZHK German Centre for Cardiovascular Research, Partner Site Rhine-Main, Bad Nauheim, Germany
[e] INSERM, ATIP-Avenir, Aix Marseille University, Marseille Medical Genetics, Marseille, France
[f] Department of Life Sciences, Goethe University, Frankfurt am Main, Germany
[g] Max Planck Institute for Heart and Lung Research, Bioinformatics and Deep Sequencing Platform, Bad Nauheim, Germany
[h] Bordeaux Imaging Center (BIC), UMS 3420 CNRS - Université de Bordeaux - US4 INSERM, Pôle d'imagerie photonique, Centre Broca Nouvelle-Aquitaine, Bordeaux, France
[i] Centre of Marine and Environmental Research (CIMA), University of Algarve, Faro, Portugal

ARTICLE INFO

Edited by Prof. Bing Yan

Keywords:
opercular bone growth
bone matrix
caudal fin and scale regeneration
xenobiotic signaling
neutrophils

ABSTRACT

Persistent and ubiquitous organic pollutants, such as the polycyclic aromatic hydrocarbon benzo[α]pyrene (BaP), represent a major threat to aquatic organisms and human health. Beside some well-documented adverse effects on the development and reproduction of aquatic organisms, BaP was recently shown to affect fish bone formation and skeletal development through mechanisms that remain poorly understood. In this work, zebrafish bone-related *in vivo* assays were used to evaluate the osteotoxic effects of BaP during bone development and regeneration. Acute exposure of zebrafish larvae to BaP from 3 to 6 days post-fertilization (dpf) induced a dose-dependent reduction of the opercular bone size and a depletion of *osteocalcin*-positive cells, indicating an effect on osteoblast maturation. Chronic exposure of zebrafish larvae to BaP from 3 to 30 dpf affected the development of the axial skeleton and increased the incidence and severity of skeletal deformities. In young adults, BaP affected the mineralization of newly formed fin rays and scales, and impaired fin ray patterning and scale shape, through mechanisms that involve an imbalanced bone remodeling. Gene expression analyses indicated that BaP induced the activation of xenobiotic and metabolic pathways, while negatively impacting extracellular matrix formation and organization. Interestingly, BaP exposure positively regulated inflammation markers in larvae and increased the recruitment of neutrophils. A direct interaction between neutrophils and bone extracellular matrix or bone forming cells was observed *in vivo*, suggesting a role for neutrophils in the mechanisms underlying BaP osteotoxicity. Our work provides novel data on the cellular and molecular players involved in BaP osteotoxicity and brings new insights into a possible role for neutrophils in inflammatory bone reduction.

1. Introduction

Polycyclic aromatic hydrocarbons (PAHs) are persistent organic pollutants (POPs) produced by incomplete combustion of organic compounds. Their presence in the environment typically results from natural events, such as volcanic activity and forest fires, and anthropogenic activity, such as car exhaust, petroleum exploration, residential waste burning and manufacturing of carbon, coal tar pitch and asphalt (Lamichhane et al., 2016; Lawal, 2017). Because they are hydrophobic and chemically stable compounds (Shin et al., 2006), PAHs are persistent in the environment and are detected in the atmosphere, water-bodies and sediments. The lipophilic nature of PAHs facilitates their accumulation in fatty tissues of aquatic organisms thus their entry in the food web, raising concerns for human health (Zhang et al., 2017; De Gelder et al., 2016). In this regard, people living in urban areas, smokers, grill and coke oven workers are daily exposed to PAHs and

* Corresponding author.
E-mail address: vlaize@ualg.pt (V. Laizé).

https://doi.org/10.1016/j.ecoenv.2021.112838
Received 2 July 2021; Received in revised form 22 September 2021; Accepted 23 September 2021
Available online 1 October 2021

several studies have revealed the presence of PAH compounds in urine, blood and breast milk (Hadrup et al., 2019; Hilton et al., 2017; Oliveira et al., 2021; Santonicola et al., 2017).

Benzo[α]pyrene (BaP) – a model compound of the PAH family – has been widely used to assess the toxic effects of this class of POPs on terrestrial and aquatic organisms. In fish, exposure to BaP can occur through dermal exposure, respiration, or consumption of contaminated prey or sediments. BaP is carcinogenic and has been included in the priority list of substances that, due to their persistence, bioaccumulation and toxicity, need to be monitored and environmentally risk assessed both in Europe and in the United States (lists are available from the European Environmental Agency at www.eea.europa.eu and from Environmental Protection Agency at www.epa.gov). In the aquatic environment, BaP concentrations range from 6.3×10^{-7} to 4.5×10^{-5} μM (Suvarapu and Baek, 2017; Moon et al., 2007; Manoli and Samara, 1999) and in some extreme cases can reach 1.9×10^{-2} μM (Zhou and Maskaoui, 2003).

Several studies have revealed the adverse effects of BaP and other PAHs on developmental, reproductive, hepatic, endocrine and immunological processes in exposed vertebrates (reviewed by Collier in et al., 2013; Williams in et al., 2015). Beside these well-documented toxic effects, BaP and other PAHs have also been shown to affect bone homeostasis (e.g., in the zebrafish *Danio rerio*, European seabass *Dicentrarchus labrax* and mouse *Mus musculus*) (Laizé et al., 2018; Danion et al., 2011; Rondelli et al., 2016; Iqbal et al., 2013) by decreasing bone formation or increasing bone resorption. Bone is a dynamic tissue undergoing constant remodeling, a process coordinated by the concerted action of osteoblasts (bone formation) and osteoclasts (bone resorption) and critical to calcium and phosphate homeostasis, micro-fracture repair, and adaptation of the skeleton to mechanical loading (Hall, 2015). Imbalanced remodeling may result in a bone with altered microarchitecture and structure (i.e., a weaker bone) and may lead to a skeleton with deformities. In humans, epidemiological studies indicate that exposure to PAHs through smoking or cooking activities can lead to bone diseases such as osteoporosis, which results in bones with reduced mineral density and prone to fractures (Al-Bashaireh et al., 2018; Chen et al., 2020; Guo et al., 2018).

In fish, such defects may affect swimming performance, impair feeding activity and consequently reducing welfare, or further increasing mortality or susceptibility to predation (Seemann et al., 2015; Boglione et al., 2013). Therefore, the osteotoxic effects of PAHs have been assessed in various teleost fishes. For example, experimental oil spills containing PAHs were found to alter the expression of transcripts encoding proteins involved in bone resorption (up-regulation) and bone formation (down-regulation) in the Atlantic cod *Gadus morhua (*Olsvik et al., 2011*)* and to decrease vertebrae mineralization in the European seabass (Danion et al., 2011). In the rainbow trout *Oncorhynchus mykiss* and the pink salmon *Oncorhynchus gorbuscha*, PAHs mixtures have been shown to increase craniofacial and spinal deformities (Carls and Thedinga, 2010; Barron et al., 2004), and 3-methylcholanthrene (another well-studied PAH compound) has been shown to increase skeletal malformations as well as decrease bone mineralization and regeneration in the zebrafish (Laizé et al., 2018). In the false kelpfish *Sebastiscus marmoratus*, BaP has been shown to alter the expression of bone marker genes related to Shh signaling, thus leading to skeletal deformities such as spinal curvature and jaw defects (He et al., 2011). BaP has also been shown to trigger transgenerational effects (F1-F3 generations) on bone of the Japanese medaka *Oryzias latipes*, in particular an increase in vertebrae compression, as well as a reduction of bone integrity and thickness, bone formation and osteoblast numbers (Seemann et al., 2015, 2017). Multigenerational deformities (F1-F2 generations) were also observed in BaP exposed zebrafish larvae, in particular in the caudal and pectoral fins and craniofacial structures (Corrales et al., 2014). Torvanger et al. (2018) recently reported a reduction in osteoblast and osteoclast activity in *ex vivo* scales of zebrafish and goldfish *Carassius auratus* after exposure to BaP.

Due to numerous technical advantages, similarities in bone biology with mammalian systems, availability of genetic tools, live imaging, and its capacity to regenerate skeletal structures, zebrafish is deemed a suitable organism for ecotoxicological studies and to investigate bone processes during development and regeneration (Fernández et al., 2018; Laizé et al., 2014). In this work, we aimed at better understanding the osteotoxic effects of BaP by assessing bone formation, mineralization and patterning in developing and regenerating zebrafish bone structures (Fernández et al., 2018; Tarasco et al., 2017; Cardeira et al., 2016; de Vrieze et al., 2014), evaluating bone cell activity using transgenic reporter lines, and quantifying xenobiotic signaling and bone marker gene expression. Following recent *in vitro* data providing evidence of interaction between neutrophils and bone forming/resorbing cells (Allaeys et al., 2011; Bastian et al., 2018; Kim et al., 2020; Sugisaki et al., 2020), their involvement in the mechanisms of BaP osteotoxicity will also be addressed.

2. Materials and methods

2.1. Ethics statement on animal experiments

Procedures involving animals were performed following the EU and Portuguese legislation for animal experimentation and welfare (Directives 86/609/CEE and 2010/63/EU; Portaria 1005/92, 466/95 and 1131/97; Decreto-Lei 113/2013). Animal handling and experimentation were performed by qualified operators accredited by the Portuguese Direçãõ-Geral de Alimentaçãõ e Veterinária (authorization no. 0421/000/000). All efforts were made to minimize pain, distress, and discomfort. Experiments were terminated (fish were returned to normal conditions or euthanized) whenever adverse effects were observed.

2.2. Chemical solutions

All chemicals were purchased from Sigma-Aldrich (St. Louis, MI, USA) unless otherwise stated. A stock solution of benzo[α]pyrene (BaP) was prepared at 31.6 mM in dimethyl sulfoxide (DMSO, 100%) and stored at −20 ºC in a glass flask. It was freshly diluted to selected concentrations prior to each experiment.

2.3. Zebrafish maintenance

Zebrafish – AB wild-type strain, and transgenic lines *Tg(Ola.Sp7:mCherry-Eco.NfsB)*^{pd46} (Singh et al., 2012), *Tg(Ola.osteocalcin:EGFP)*^{hu4008} (Knopf et al., 2011) and *TgBAC(mpx:GFP)*^{i114} (Renshaw et al., 2006), referred to as *Tg(sp7:mCherry)*, *Tg(osteocalcin:GFP)* and *Tg(mpx:GFP)* – were maintained in a ZebTEC (Tecniplast, Buguggiate, Italy) recirculating system with controlled water parameters (i.e., temperature 28 ± 0.1 °C, pH 7.5 ± 0.1, conductivity 700 ± 50 μS, ammonia and nitrites lower than 0.1 mg/L, nitrates at 5 mg/L) under a 14–10 h light-dark photoperiod. System water was prepared by adding, using an automatic dosing system, salt (35 g/L; Instant Ocean, Blacksburg, VA, USA) and sodium bicarbonate (30 g/L; Fisher Scientific, MA, USA) to reverse osmosis treated water in order to achieve the desired pH and conductivity set in the ZebTEC system. System water was automatically replaced (10%) every day. Fish were fed twice a day with *Artemia* nauplii (strain AF480 from INVE Aquaculture, Dendermonde, Belgium) and ZEBRAFEED microdiet (Sparos Lda, Olhão, Portugal) *ad libitum*.

2.4. Experimental design

Parameters (e.g., developmental stages, duration of BaP exposure, frequency of treatment renewals, endpoints for each assay) associated with zebrafish experimentation are summarized in Fig. 1.

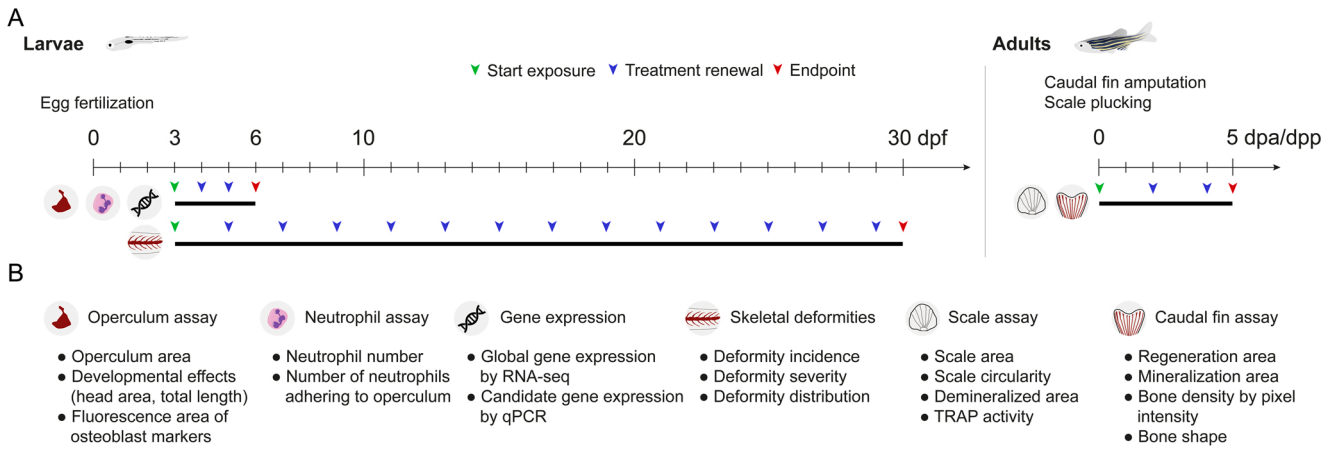

Fig. 1. Experimental design of the zebrafish assays used to assess the effects of BaP exposure on bone throughout development and regeneration. (A) Time course of the *in vivo* assays performed using larval (*left panel*) and adult stages (*right panel*), including information on the onset of BaP exposure, the schedule for treatment renewals and endpoint collection. *dpf*, days post-fertilization; *dpa*, days post-amputation; *dpp*, days post-plucking. (B) Biological parameters evaluated at each endpoint for each assay. For interpretation of the references to color in this figure legend, the reader is referred to the web version of this article.

2.5. Operculum growth assay

Sexually mature zebrafish aged between 6 and 18 months were crossed (1:2 male:female sex ratio) and fertilized eggs (approximately 200 eggs per breeding event) were transferred into a 1-L nursing tank (Tecniplast) and cultured under static water conditions. Methylene blue (0.0002% w/v) was added to prevent fungal growth. At 3 days post-fertilization (dpf), larvae were randomly transferred into borosilicate glass flasks (15 larvae in 10 mL of fish water) and exposed to BaP at concentrations ranging from 0.01 to 31.6 μM, calcitriol (1α,25-dihydroxyvitamin D_3) at 10 pg/mL, or DMSO and ethanol (vehicle for BaP and calcitriol, respectively) at 0.1%. About 70% of the fish water was renewed daily until the end of the treatment. At 6 dpf, larvae were euthanized with a lethal dose of anesthetic (tricaine; MS222), stained for 15 min at room temperature with 0.01% alizarin red S (AR-S; pH 7.4) prepared in Milli-Q water (Merck Millipore, Darmstadt, Germany), and washed twice with Milli-Q water for 5 min (method adapted from Bensimon-Brito et al., 2016). Stained larvae were placed in a lateral plane on top of a 2% agarose gel, imaged and analyzed. To evaluate the effects of BaP on the expression of immature and mature osteoblast markers, larvae of the transgenic zebrafish lines *Tg(sp7:mCherry)* and *Tg(osteocalcin:GFP)* were exposed to 1 μM BaP and 0.1% DMSO from 3 to 6 dpf. The fluorescence area was measured and corrected by the area of the operculum stained with either 0.2% calcein or 0.01% AR-S in combination with *Tg(sp7:*mCherry*)* and *Tg*(*osteocalcin:GFP)* transgenes, respectively. Images were acquired using a MZ10F fluorescence stereomicroscope (Leica, Wetzlar, Germany) equipped with either mCherry (ex: ET560/40x; em: ET630/75 m) or GFP (ex: ET470/40x; em: ET525/50m) filters and a DFC7000T color camera (Leica). Images were acquired using the following parameters: exposure time 600 ms, gamma 1.00, image format 1920 × 1440 pixels and binning 1 × 1. Experimental settings and morphometric analysis were performed as described by Tarasco et al. (2017) using ZFBONE ImageJ toolset (Tarasco et al., 2020).

2.6. Axial skeleton development assay

For this assay, fish were exposed to BaP from 3 dpf (onset of bone development) until 30 dpf (when all the bony structures of the axial skeleton are fully developed). 3-dpf zebrafish larvae were randomly placed into 1.5-L EPA-certified soda-lime glass jars (Thermo Fisher Scientific, Waltham, MA, USA) at a density of 100 larvae per jar and exposed for 27 days to BaP at concentrations ranging from 0.01 to 10 μM, or DMSO at 0.1%. About 80% of the fish water was renewed every second day until the end of the treatment. At 30 dpf, larvae were euthanized with a lethal dose of anesthetic (see above) and stained with 0.05% AR-S prepared in 1% potassium hydroxide, cleared using 1% potassium hydroxide and preserved in increasing series of glycerol up to 75%, as described by (Walker and Kimmel, 2007). The incidence, typology (such as shape variation, anomalous supernumerary elements, fusions or platyspondyly) and charge of deformities in the axial skeleton were determined through stereomicroscopy observation and structures classified according to (Bird and Mabee, 2003). Representative images were acquired using a LSM 800 confocal microscope (Zeiss, Oberkochen, Germany) equipped with a 10×/0.45 M27 objective. Images were acquired at 1024 × 1024 pixels using 15% laser power at 561 nm, acquisition speed = 8.26 μs, mCherry channel (λex: 587, λem 610) and a GaAsP detector set to gain = 650 V and digital gain = 0.3. Z slices were recorded at 4 μm per section and adjusted to cover the full depth of region of interest.

2.7. Caudal fin regeneration assay

Young adult zebrafish (3-months old) were anesthetized with 0.6 mM tricaine (MS222) and placed on the stage of a stereomicroscope. Caudal fin was carefully deployed, flattened and amputated 1–2 segments anterior to the bifurcation of the most peripheral branching lepidotrichia using a sterile scalpel in a single downward movement. Fish were allowed to recover and then placed randomly into a 1.5-L EPA-certified soda-lime glass jar (8 fish per jar) containing water from the rearing system and maintained at 33 ± 0.1 °C. Fish regenerating their caudal fin were exposed for 5 days to BaP at concentrations ranging from 0.01 to 10 μM, or DMSO at 0.1%. About 80% of the fish water was renewed every second day until the end of the experiment. At 5 days post-amputation (dpa), fish were stained for 20 min with 0.01% AR-S (pH 7.4, prepared in system water) and euthanized with a lethal dose of anesthetic (see above). Images were acquired using a Leica MZ10F fluorescence stereomicroscope equipped with a mCherry filter and a Leica DFC7000T color camera, as described above. Caudal fin regeneration, *de novo* bone formation and patterning were assessed through the morphometric analysis of regenerated areas as described by Cardeira et al. (2016) and using ZFBONE ImageJ toolset (Tarasco et al., 2020). The percentage of fin bifurcation is defined as the ratio between the distance from the stump to the bifurcation point and the distance from the stump to the ray tip. For each fin, 8 rays were measured (4 rays for each fin lobe) and averaged. The mineral density of newly formed bone was assessed in regenerating fin (5 fins per condition) exposed to 1 μM BaP or 0.1% DMSO, and scanned with a SkyScan 1272 high-resolution

3D X-ray microscope based on micro computed tomography (micro-CT) technology (Bruker, Kontich, Belgium) using a 60-kV voltage, a 166-μA current and a 0.25-mm thick aluminum filter. For each sample, 800 projections with an isotropic voxel size of 3 μm were acquired over a rotation range of 360° with a rotation step of 0.45°. The cross-sectional images (4904 × 4904 pixels) were reconstructed from the X-ray projections using the NRecon software v1.6.10.2 (Bruker). During reconstruction, the following parameters were used: compensate for misalignment (82), smoothing (2) and beam hardening (50%). Images were imported in FIJI software for background subtraction (Rolling ball radius: 25 pixel) and stack merging through average projection. The pixel intensity of 8 lepidotrichia per fin was assessed using ZFBONE ImageJ toolset (Tarasco et al., 2020).

2.8. Scale regeneration assay

Young adult zebrafish (3-months old) were anesthetized with 0.6 mM tricaine and placed on the stage of a stereomicroscope. Ontogenetic scales (around 20–30 per fish) were carefully plucked from the left flank of the body using thin stainless-steel forceps. Fish were allowed to recover and then randomly placed into a 1.5-L EPA-certified soda-lime glass jar (8 fish per cup) containing water from the rearing system and maintained at 33 ± 0.1 °C. Fish were exposed for 5 days to BaP at concentrations ranging from 0.01 to 10 μM, or DMSO at 0.1%. About 80% of the fish water was renewed every second day until the end of the experiment. At 5 days post-plucking (dpp), fish were euthanized with a lethal dose of anesthetic (see above) and regenerating scales were collected (same procedure as above), washed in phosphate-buffered saline (PBS) and fixed for 30 min at 4 °C in 4% formaldehyde (prepared in PBS, pH 7.4). Scales were dehydrated through ice-cold increasing series of ethanol up to 100% and preserved at −20 °C. Osteoclast enzymatic activity was assessed through tartrate-resistant acid phosphatase (TRAP) staining. Scales were rehydrated, washed with PBS and incubated at room temperature in a 0.1 M sodium acetate buffer (pH 5.1) containing 50 mM of L(+)-tartaric acid. Scales were then incubated in the dark until TRAP signal was revealed (approximately 1 h) using naphthol AS-TR phosphate as substrate and hexazotized pararosaniline, as described by Witten (1997). Scales were rinsed twice in water and then preserved through an increasing series of glycerol (Biochem Chemopharma, Cosne sur loire, France) up to 75% until image acquisition.

Mineral deposition was assessed in von Kossa stained scales. Briefly, scales were rehydrated, washed with PBS and incubated for 1 h in 5% silver nitrate, under UV light. Scales were then rinsed with distilled water for 5 min and immersed for 5 min in 2.5% sodium thiosulfate. Finally, scales were rinsed thoroughly with distilled water and preserved in increasing series of glycerol up to 75% until image acquisition. Bright-field images of TRAP and von Kossa stained scales were acquired using a SteREO Lumar.V12 stereomicroscope and the following parameters: 16-bit RGB image, exposure time 100 ms, gamma 1.00, image format 1384 × 1040 pixel and binning 1 × 1. Scales area, circularity, osteoclast activity and mineral deposition were assessed throughout morphometric analysis using ZFBONE ImageJ toolset (Tarasco et al., 2020).

2.9. RNA preparation and gene expression analysis

Total RNA was isolated from 6-dpf zebrafish larvae exposed to 1 μM BaP or 0.1% DMSO (4 biological replicates per condition, prepared from pools of 30 larvae) using NZYol (NZYTech, Lisbon, Portugal) and treated with RQ1 RNase-Free DNase (Promega, WI, USA) to avoid contamination by genomic DNA. RNA integrity and quantity were confirmed using an Experion Automated Electrophoresis system (Bio-Rad, Hercules, CA, USA) and only RNA with a RIN > 9.8 was further used. RNA-seq – a single readout of the pooled replicates – was first used to gain insights into the molecular mechanisms involved in BaP osteotoxicity; qPCR analysis of the 4 biological replicates was later used to confirm the differential expression of candidate genes.

2.9.1. Gene expression analysis by RNA-seq

RNA and library preparation integrity were verified with LabChip Gx Touch 24 (PerkinElmer). 200 ng of total RNA was used as input for VAHTS Stranded mRNA-seq Library preparation following manufacture's protocol (Vazyme). Sequencing was performed on NextSeq500 instrument (Illumina) using v2 chemistry, resulting in average of 27 M reads per library with 1x75bp single end setup. The resulting raw reads were assessed for quality, adapter content and duplication rates with FastQC (Andrews, 2010). Trimmomatic version 0.38 was employed to trim reads after a quality drop below a mean of Q20 in a window of 5 nucleotides (Bolger et al., 2014). Only reads between 30 and 150 nucleotides were cleared for further analyses. Trimmed and filtered reads were aligned versus the Ensembl zebrafish genome version DanRer11 (GRCz11.92) using STAR 2.6.1d with the parameter "–outFilterMismatchNoverLmax 0.1" to increase the maximum ratio of mismatches to mapped length to 10% (Dobin et al., 2013). The number of reads aligning to genes was counted with featureCounts 1.6.3 tool from the Subread package (Liao et al., 2014). Only reads mapping at least partially inside exons were admitted and aggregated per gene. Reads overlapping multiple genes or aligning to multiple regions were excluded. Gene ontology analyses were performed using PANTHER (Protein Analysis THrough Evolutionary Relationships) and pathway enrichment was determined using REACTOME classification system. Ensembl zebrafish gene IDs of differentially expressed genes exhibiting a fold change greater than 2 and lower than 0.5 in RNA-seq dataset were used as input data. Over-representation was tested using Bonferroni correction for multiple testing. In this regard, the number of differentially expressed genes (in this study) is compared to the zebrafish reference list (all genes in the database) and P-value is calculated using the binomial test to determine whether the over- or under- representation is significant or not. RNA-seq data have been deposited in NCBI Gene Expression Omnibus under the GEO Series accession number GSE174529 (https://www.ncbi.nlm.nih.gov/geo/).

2.9.2. Gene expression analysis by qPCR

Total RNA (1 μg) was reverse-transcribed for 1 h at 37 °C using M-MLV reverse transcriptase (Invitrogen, Carlsbad, CA, USA), oligo-d(T) primer and RiboLock RNase inhibitor (Thermo Fisher Scientific). All quantitative real-time PCR (qPCR) reactions were performed using SensiFAST SYBR Hi-ROX kit (Meridian Bioscience, Cincinnati, OH, USA), 10 μM of gene-specific primers (Supplementary Table 1) and 1:10 dilution of reverse-transcribed RNA, in a CFX Connect Real-Time PCR detection system (Bio-Rad). PCR amplification was as follows: an initial denaturation step of 2 min at 95 °C and 40 cycles of amplification (10 s at 95 °C and 20 s at 65 °C). Efficiency of amplification was above 95% for all primer sets. Levels of gene expression were calculated using the ΔΔCt comparative method (Pfaffl, 2001) and normalized using the average of two housekeeping genes (i.e., *eef1a1l1* and *rps18*) previously validated in zebrafish larvae (Tang et al., 2007).

2.10. Neutrophil quantification

Adults of the *TgBAC(mpx:GFP)*^{i114} line (where neutrophils are labeled with green fluorescence) were crossed and fertilized eggs (approximately 200 eggs) were transferred into a 1-L nursing tank (Tecniplast) with static water conditions. Methylene blue (0.0002% w/v) was added to prevent fungal growth. At 3 dpf, larvae were randomly transferred into borosilicate glass flasks (30 larvae in 25 mL of fish water) and exposed to 1 μM BaP or 0.1% DMSO. About 70% of the fish water was renewed daily until the end of the treatment. At 6 dpf, larvae were euthanized with a lethal dose of anesthetic (see above), then stained for 15 min at room temperature with 0.01% AR-S and washed twice with fish water for 5 min. Stained larvae were embedded in 1% low melting agarose for imaging. Representative images were acquired

using an Axio Observer.Z1.7 spinning disk confocal microscope (Zeiss, Oberkochen, Germany) equipped with a 40×/1.1 W Korr UV VIS IR water immersion objective. Images were acquired at 804 × 804 pixels using 8% laser power at 488 nm excitation with 50 ms exposure time for EGFP channel and 30% laser power at 587 nm excitation with 100 ms exposure time for mCherry channel. Z slices were recorded at 1 μM per section and adjusted to cover the depth of the operculum.

2.11. Statistical analysis

Data were analyzed using Prism version 8.2.1 (GraphPad Software, Inc. La Jolla, CA, USA). One-way analysis of variance (ANOVA) followed by Dunnett's multiple comparison test or an unpaired *t*-test with Welch's correction were used for data sets presenting a normal distribution. Kruskal-Wallis test followed by Dunn's multiple comparison test was used for data sets that did not follow a normal distribution. A chi-squared test, 1degree of freedom, was used to analyze data sets related to skeletal deformity. In all cases, differences were considered significant for $p < 0.05$. Blind analyses were performed whenever possible to reduce the bias associated to experimenters.

3. Results

3.1. Benzo[α]pyrene impairs operculum growth by affecting osteoblast maturation

To understand the effect of BaP on bone formation, zebrafish larvae were exposed for 3 days to BaP (from 0.01 to 31.6 μM) and operculum area, head area and standard body length were determined through morphometric analysis. Head area was used to normalize the area of the operculum while standard body length was assessed to evaluate larvae developmental impairment. We observed that only BaP concentrations higher than 0.1 μM inhibited operculum growth (Fig. 2A). When the corrected operculum area of BaP-treated larvae was compared with the

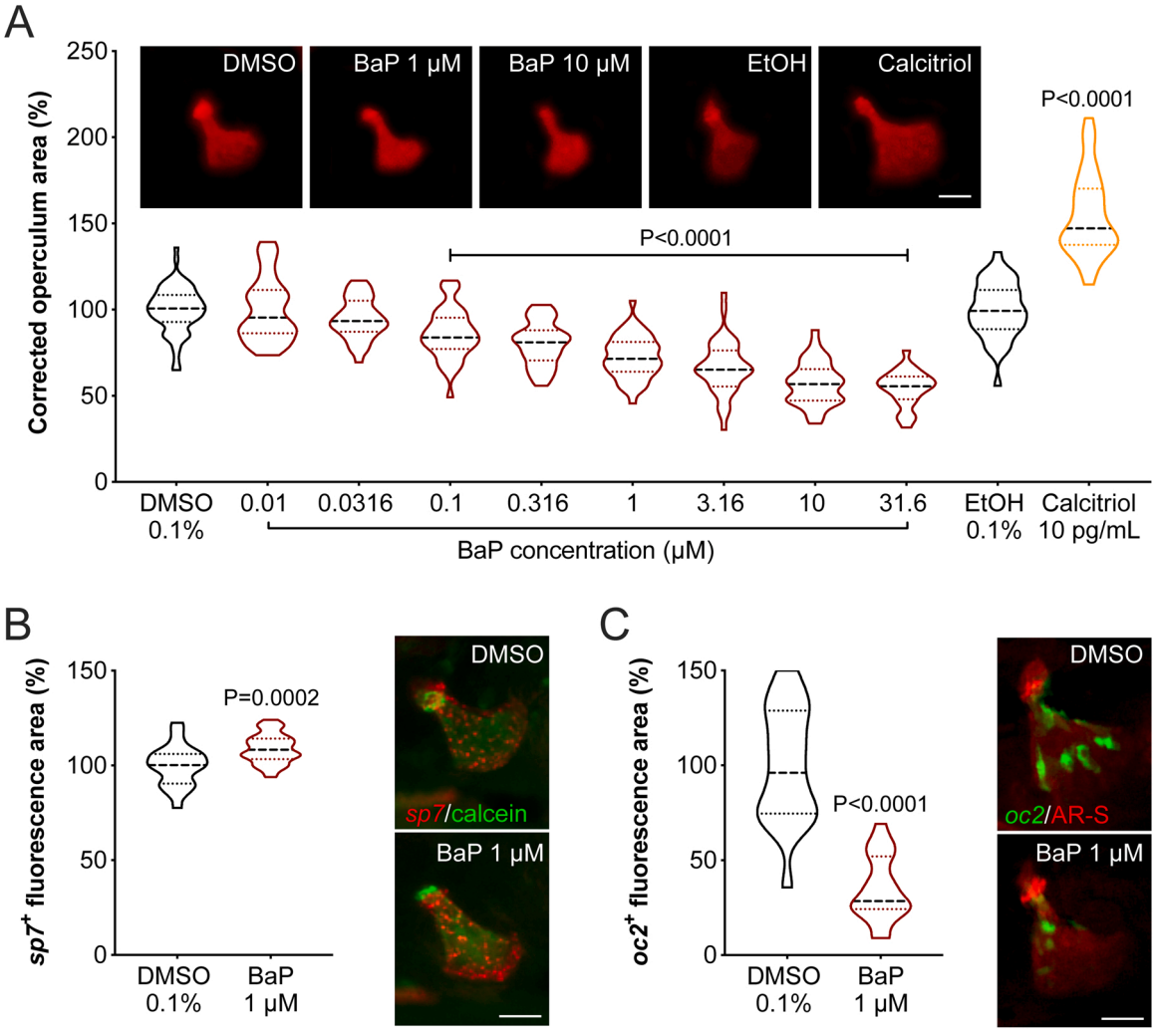

Fig. 2. (A) Operculum growth in zebrafish larvae exposed to increasing concentrations of BaP from 3 to 6 dpf. Regions of interest (operculum and head area) were determined through the morphometric analysis of AR-S stained bone structures imaged by fluorescence microscopy. Representative images of AR-S stained operculum are presented on the top of the graph (background was removed using image processing software to highlight operculum structure). Dimethyl sulfoxide (DMSO) and ethanol (EtOH) were used as vehicle for BaP and calcitriol, respectively. Scale bar is 50 μm. P-value calculated using one-way ANOVA followed by Dunnett's multiple comparison test for BaP/DMSO and Student's *t*-test for calcitriol/EtOH. Values are presented as median and quartiles ($n \geq 25$). (B, C) Expression of osteoblast marker genes in the operculum of zebrafish larvae exposed to 1 μM BaP or 0.1% DMSO from 3 to 6 dpf. (B) osterix (sp7), a marker of immature osteoblasts, appears in red in the *Tg(Ola.Sp7:mCherry-Eco.NfsB)*^{pd46} line; operculum is counter-stained with calcein. (C) osteocalcin (oc2), a marker of mature osteoblasts, appears in green in the *Tg(Ola.osteocalcin:EGFP)*^{hu4008} line; operculum is counter-stained with AR-S. Representative images of the operculum are presented on the right side of the respective graph. Scale bar is 50 μm. P-value calculated using Student's *t*-test. Values are presented as median and quartiles ($n \geq 21$). For interpretation of the references to color in this figure legend, the reader is referred to the web version of this article.

control value (0.1% DMSO), reductions of 13.8 ± 2.7% and 45.5 ± 3.2% were observed at the lowest effective concentration (0.1 μM) and at the highest non-lethal concentration (31.6 μM), respectively, following a dose-dependent response. In all experiments, the corrected operculum area of calcitriol-treated larvae (positive control) increased by 54.5 ± 4.7%, confirming the fitness of the embryo batch and the responsiveness of the assay. Head area and body standard length were slightly reduced at the two highest concentrations (Supplementary Fig. 1), indicating that BaP affected larval development in a more general manner at concentrations higher than 10 μM. To gain insights into the mechanisms underlying BaP effects on bone cells and their maturation, the expression of marker transgenes for immature and

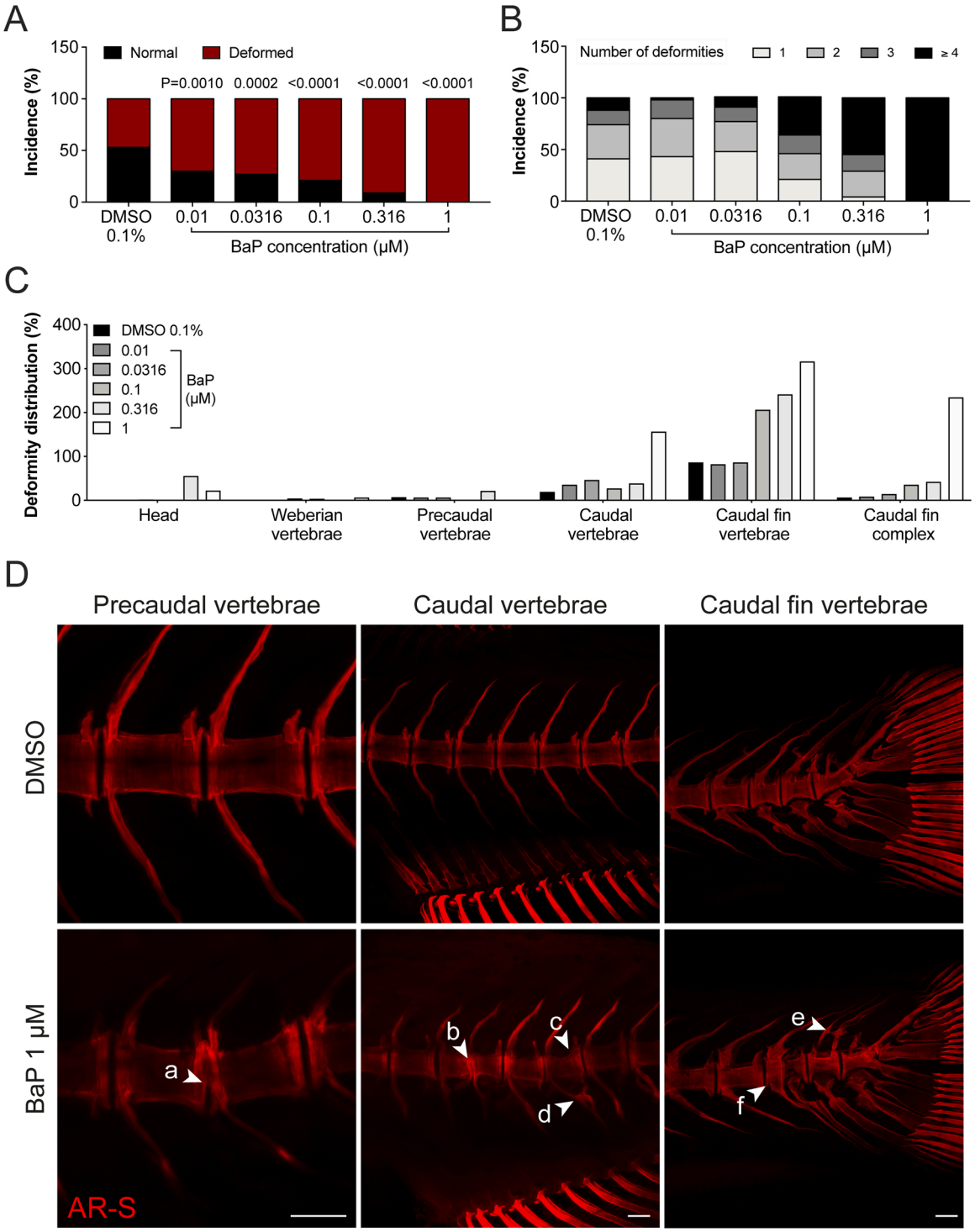

Fig. 3. Deformities in the axial skeleton of 30 dpf juvenile zebrafish exposed to increasing concentration of BaP throughout their development. (A) Percentage of normal and deformed zebrafish. (B) Percentage of deformities per deformed larvae. (C) Distribution of the deformities along the axial skeleton. Deformed structures of each individual were summed and divided by the number of fish. (D) Representative fluorescence images of AR-S stained skeletal structures exposed to 0.1% DMSO or 1 μM BaP. Arrowheads point to: a, partially fused vertebrae; b, fused vertebrae; c, deformed vertebrae; d, fused hemal arches; e, ectopic mineralization; f, platyspondyly. Scale bar is 100 μm. P-value calculated using chi-squared test, 1 degree of freedom. n ≥ 65, except for BaP 1 μM (n = 18). For interpretation of the references to color in this figure legend, the reader is referred to the web version of this article.

mature osteoblasts (i.e., *Tg(sp7:mCherry)* and *Tg(osteocalcin:GFP)*, respectively) was monitored in the operculum of larvae exposed to 1 μM BaP for 3 days. The intra-operculum fluorescent signal area increased by 8.80 ± 2.27% (Fig. 2B) for *Tg(sp7:mCherry)* and decreased by 64.89 ± 7.61% (Fig. 2C) for *Tg(osteocalcin:GFP)*, when compared to control, suggesting that BaP impairs osteoblast maturation, i.e., by blocking the transition of immature osteoblasts (*sp7*-positive cells) to a mature state (*osteocalcin*-positive cells). It is worth to mention that the operculum area determined by calcein/AR-S staining was also reduced in BaP-treated versus control transgenic larvae (Supplementary Fig. 2) indicating that results with reporter lines relate to the morphological phenotype observed in wild-type line.

3.2. Benzo[α]pyrene affects zebrafish axial skeleton development

To assess the effect of BaP on skeletogenesis, the axial skeleton of zebrafish juveniles exposed for 27 days to BaP (from 0.01 to 10 μM) was evaluated for the incidence of deformed fish, the number of deformities per fish and their distribution along the axial skeleton. At the two highest concentration (i.e., 3.16 and 10 μM) all the fish died after 5 days of exposure and no data was retrieved. Fish exposed to the other concentrations presented an increasing incidence of deformities, starting from 70% at 0.01 μM BaP and reaching 100% at 1 μM BaP (Fig. 3A). An increasing number of skeletal malformations correlated to increasing concentrations of BaP. We observed a minimum of 4 deformed axial skeletal structures per fish upon exposure to 1 μM BaP (Fig. 3B). BaP affected several structures of the axial skeleton and several types of deformities were reported, e.g., partial/total fusion of the vertebrae or neural/hemal arches and malformations of the operculum, urostyle, parhypural and hypurals (Fig. 3D). The caudal vertebrae, caudal fin vertebrae and caudal fin complex were the most affected regions. Only the highest concentrations of BaP (0.316 and 1 μM) affected skeletal structures in the head region (Fig. 3C). This data confirms the osteotoxic effect of BaP during skeletal development upon chronic exposure.

3.3. Benzo[α]pyrene impairs bone mineral density and patterning

To evaluate the effect of BaP on *de novo* bone formation, adult zebrafish were finectomized and exposed for 5 days to BaP (from 0.01 to 10 μM). Caudal fin regeneration, *de novo* bone formation and ray patterning were assessed through morphometric analysis. Fish exposed to 1, 3.16 and 10 μM BaP showed a reduction in regenerated caudal fin tissues of 19.10 ± 5.7%, 21.10 ± 6.0% and 30.50 ± 6.4% over control, respectively (Fig. 4A). Lower concentrations also triggered a decrease in fin regeneration although to an extent not statistically significant. While none of the concentrations tested altered the extent of *de novo* bone formation (Fig. 4B), we observed that the patterning of newly formed rays was strongly affected at these concentrations. Rays bifurcated earlier (24.2 ± 5.0%) in BaP-treated versus control fish, modifying the shape of the fin through the proximalization of ray branching (Fig. 4C, D). Bone mineral density was then evaluated by micro-computed tomography (μCT) in adult zebrafish regenerating their caudal fins upon exposure to 1 μM BaP for 5 days. Pixel intensity was assessed in μCT images of regenerating rays (Fig. 4F). Pixel intensity was lower in BaP-treated versus control fish, from the amputation plane along all the ray length (Fig. 4E) and the assessment of the total area under the intensity curve showed a reduction of 29.81 ± 4.90% (Fig. 4G), indicating an impairment of *de novo* bone mineralization.

3.4. Benzo[α]pyrene inhibits scale mineralization and increase osteoclast activity during regeneration

To validate BaP inhibition of bone mineralization during regeneration, we assessed scale area, circularity, TRAP signal and demineralized area in adult zebrafish regenerating scales upon exposure to BaP (from 0.01 to 10 μM) for 5 days. All parameters were affected by BaP at all tested concentrations (Fig. 5E). We observed that scale area was reduced by 36.84 ± 3.03% and 54.41 ± 4.24% at the lowest (0.01 μM) and highest (10 μM) concentrations, respectively (Fig. 5A) indicating a reduction in mineralization. Scale circularity was reduced by 2.68 ± 0.47% and of 6.52 ± 0.59% at the lowest and highest concentrations, respectively, further confirming their affected morphology (Fig. 5B). TRAP signal was increased by 920.10 ± 330.90% and 2884.00 ± 406.30% at the lowest and highest concentrations, respectively (Fig. 5C). Finally, demineralized area was increased by 86.28 ± 25.61% and 226.90 ± 43.74% at the lowest and highest concentrations, respectively (Fig. 5D). Together, our data show that BaP decreases bone formation while increasing osteoclast activity during scale regeneration.

3.5. Analysis of gene expression in BaP-treated larvae

To understand the molecular mechanisms behind BaP osteotoxic effects, 3-dpf larvae were exposed for 3 days to 1 μM BaP and their transcriptome was first determined by RNA-seq and compared to that of larvae exposed to 0.1% DMSO. Note that RNA-seq analysis was based on a single readout (pooled replicates) for each condition, to get insights into gene networks involved. A selection of differentially expressed genes was further analyzed by qPCR using the 4 biological replicates. Analysis of differentially expressed genes revealed that pathways related to xenobiotic response (e.g., glutathione conjugation, phase II conjugation of compounds, phase I functionalization of compounds, metabolism and biological oxidations) and to extracellular matrix degradation, formation and organization (e.g., collagen chain trimerization, collagen synthesis, formation and degradation, ECM degradation and formation, activation of metalloproteinases) were enriched in BaP-treated larvae. Interestingly, pathways related to neutrophil metabolism (e.g., neutrophil degranulation) were also enriched in BaP-treated larvae (Supplementary Fig. 3). The most enriched biological processes were related to xenobiotic response such as cellular detoxification and response to toxic substances, metabolic processes, and ECM organization (Supplementary Fig. 4).

To confirm RNA-seq data, the expression of several marker genes was assessed by qPCR (Fig. 6). We observed that expression of xenobiotic nuclear receptors and transcription factors (*ahr2*, *nr1i2* and *nr1i2 X2*) was up-regulated in BaP-treated larvae by 1.44, 1.91 and 1.53 respectively. Similarly, Phase I and II metabolizing enzymes (*cyp1a* and *gstp1*) were also up regulated by 46.90 and 7.56 folds, respectively. In contrast, while the expression of osteoblast differentiation marker genes (*runx2b*, *sp7*, and *bmp2b*) was not affected upon BaP exposure, expression of those involved in ECM mineralization (*oc2,* also known as *bglapl,* and *spp1*) was down regulated by 1.40 and 1.56 fold, respectively. Osteoblast signaling receptor (*vdrb*) was up regulated by 1.14 fold. Additionally, the expression of collagenous ECM components (*col1a1a*, *col2a1a* and *col10a1a*) was also down regulated by 1.92, 1.82 and 2.33 fold while *alpl* expression was up regulated by 1.19 fold. Expression of genes involved in osteoclastogenesis (*acp5a*, *acp5b*, *ctsk* and *fosab*) was up regulated in BaP-treated larvae by 2.20, 2.00, 1.70 and 1.82 fold, respectively, similarly to genes involved in osteoclast activity/ECM degradation (*mmp9* and *mmp13*) which were strongly up regulated by 7.53 and 10.67 fold, respectively. Inflammation and neutrophils marker genes (*il-6*, *il-1β*, *mpx* and *lyz*) were also upregulated by 1.50, 4.50, 3.00 and 2.80 fold, respectively. In a general manner, the expression levels of selected marker genes determined by qPCR confirmed pathway enrichment revealed by transcriptomic analysis.

3.6. Neutrophil recruitment and their interaction with bone increases upon BaP exposure

Our data showed an increase in expression of inflammation and neutrophil marker genes upon BaP exposure, and following recent *in vitro* studies (Allaeys et al., 2011; Bastian et al., 2018; Kim et al., 2020;

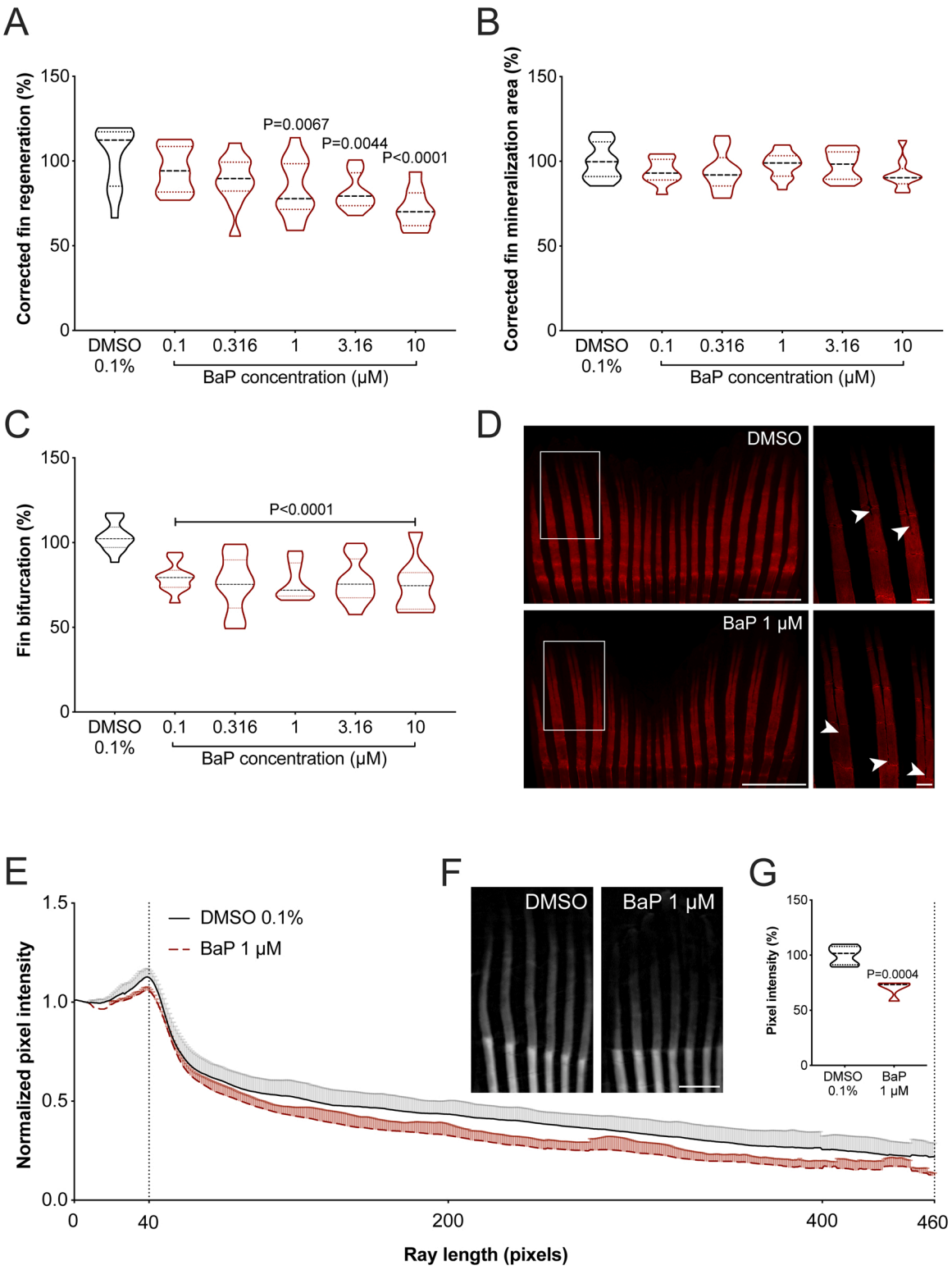

Fig. 4. Regeneration of the caudal fin in adult zebrafish exposed to increasing concentrations of BaP for 5 days after finectomy. (A) Caudal fin tissue regeneration, (B) *de novo* bone formation and (C) ray bifurcation was assessed through morphometric analysis of the fin structures in bright-field and fluorescence images. Fin bifurcation corresponds to the ratio between the distance from the stump to the bifurcation point / distance from stump to ray tip (D) Representative images of the regenerating caudal fin rays exposed to 0.1% DMSO or 1 μM BaP. Magnification of the boxed area is presented in the right panel. Arrowheads point to ray bifurcation point. Scale bar is 1 mm in left panels and 0.1 mm in right panels. P-value calculated using one-way ANOVA followed by Dunnett's multiple comparison test. Values are presented as median and quartiles ($n \geq 9$). (E-G) Density of regenerating caudal fin rays from adult zebrafish exposed to BaP for 5 days after finectomy assessed through ray pixel intensity micro–computed tomography (μCT) images. (E) Averaged normalized pixel intensity along regenerated rays from 40 (amputation plane) to 460 pixels. (F) Representative μCT images of the regenerating caudal fin rays exposed to 0.1% DMSO or 1 μM BaP. Scale bar is 1 mm. (G) Area under curve (40–460 pixels). P-value calculated using Student's *t*-test. Values are presented as median and quartiles ($n = 5$). For interpretation of the references to color in this figure legend, the reader is referred to the web version of this article.

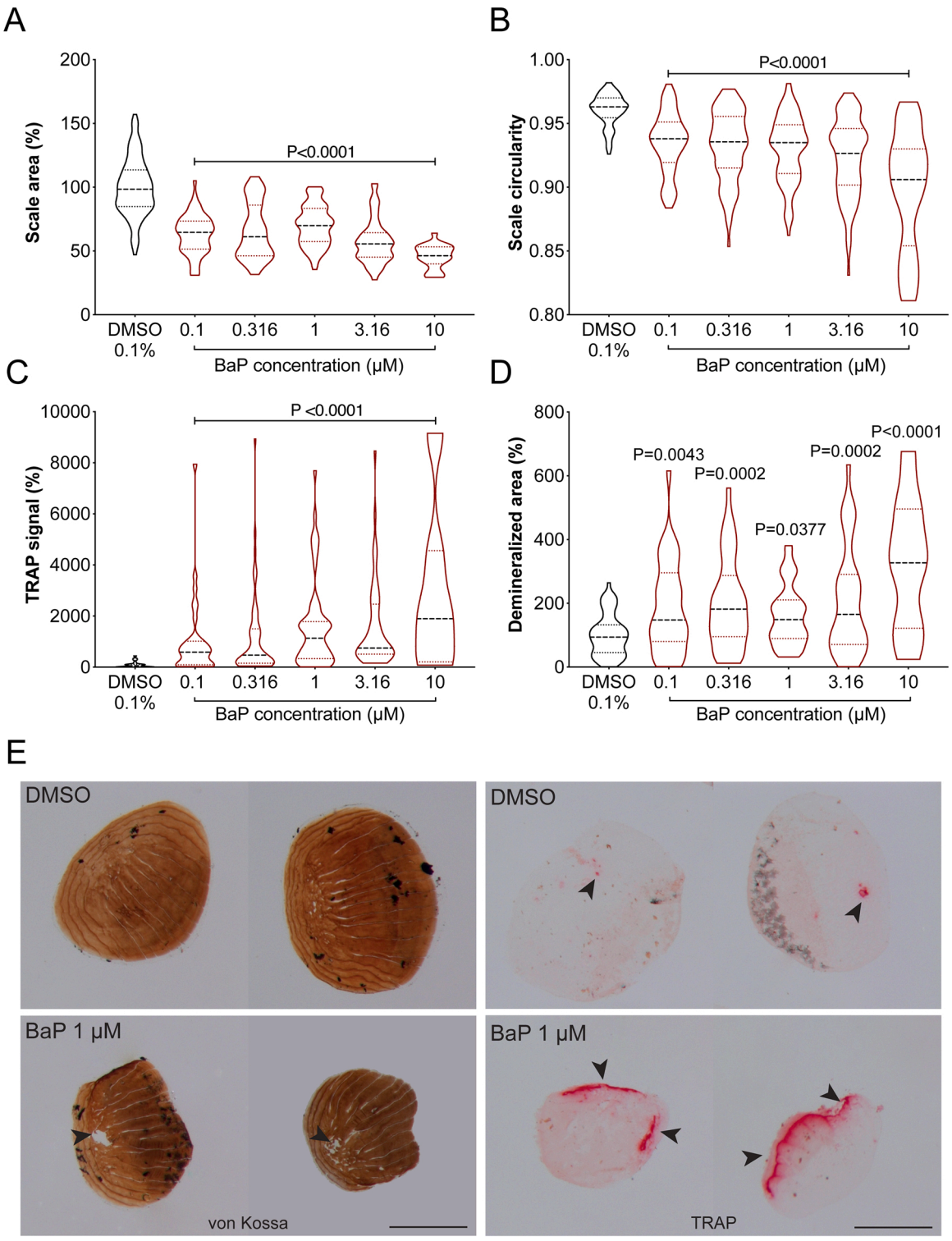

Fig. 5. Morphology, mineral content and osteoclast activity of regenerating scales from adult zebrafish exposed to increasing concentration of BaP for 5 days after plucking. (A) Scale area and (B) circularity were assessed through morphometric analysis of regenerating scales in bright-field images. (C) Osteoclast activity was assessed through TRAP (Tartrate-Resistant Acid Phosphatase) staining while (D) mineral content was evaluated through von Kossa staining. (E) Representative images of von Kossa (left panels) and TRAP (right panels) stained scales collected from adults exposed to either 0.1% DMSO or 1 μM BaP. Arrowheads point to demineralized areas or regions of TRAP signal. Scale bar is 0.5 mm. P-value calculated using Kruskal-Wallis test followed by Dunn's multiple comparisons test for TRAP activity and one-way ANOVA followed by Dunnett's multiple comparison test for scale area, scale circularity and demineralized area. Values are presented as median and quartiles ($n \geq 20$; $n = 9$ at BaP 10 μM in Demineralized area). For interpretation of the references to color in this figure legend, the reader is referred to the web version of this article.

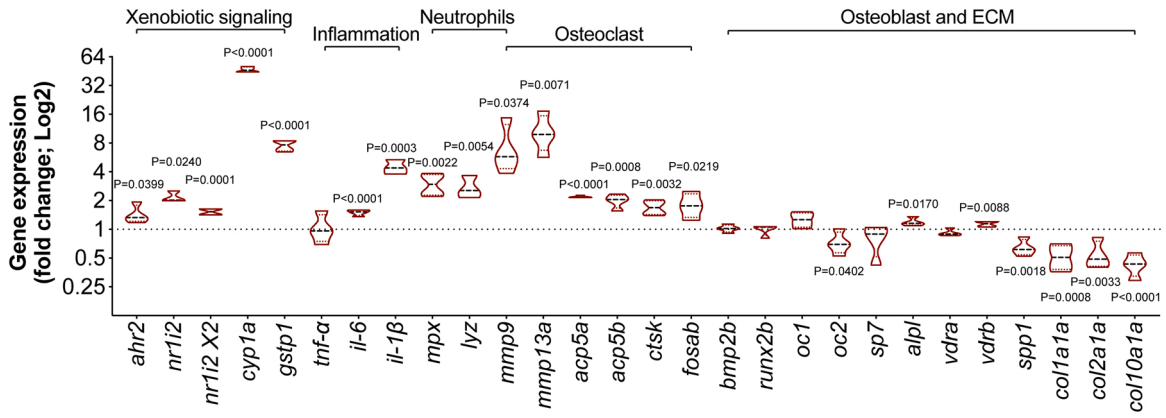

Fig. 6. Gene expression levels in zebrafish larvae exposed to 1 μM BaP from 3 to 6 dpf. The averaged expression of *eef1a1l1* and *rps18* housekeeping genes was used to normalize gene expression levels. P-value calculated using Student's *t*-test. Values are presented as median and quartiles expressed in Log2 over the control (0.1% DMSO) (n = 4).

Sugisaki et al., 2020) suggesting that neutrophils can interact with bone cells, we assessed the number of neutrophils and their interaction with the developing operculum in *Tg(mpx:GFP)* larvae exposed for 3 days to 1 μM BaP. The number of mpx:GFP positive neutrophils was significantly increased in BaP-treated larvae (Supplementary Fig. 5). This phenotype was particularly strong in the region of the trunk above the hematopoietic tissue, where neutrophil population was 2.5 times larger in BaP-treated fish than in controls (Fig. 7A, B). Confocal microscopy showed that the number of neutrophils observed at the surface of the opercular bone doubled in larvae exposed to BaP (Fig. 7C, D). A closer look at these images revealed that BaP-treated larvae presented fewer cases of operculum without neutrophils (17.78 ± 9.33%) and more cases of operculum with a single neutrophil (7.26 ± 5.16%). Similarly, while control fish opercular bones had a maximum of two neutrophils on their surface simultaneously, 10.52 ± 3.17% of larvae exposed to BaP had more than three neutrophils on the operculum surface (Fig. 7E). This observation suggests that neutrophils can interact with bone structures and may play a role in BaP osteotoxic effect.

4. Discussion

In this study, several zebrafish *in vivo* systems were used cooperatively to assess benzo[a]pyrene osteotoxicity during bone development and regeneration. A short exposure (3 days) to BaP impaired the growth of the opercular bone and decreased osteoblast differentiation during larval development. A long exposure (27 days) to BaP affected the development of the axial skeleton, increasing incidence, charge, and severity of skeletal deformities. During regeneration, BaP affected the mineralization of newly formed fin rays and scales, while it impaired fin ray patterning and scale shape. Expression data indicated that BaP activated xenobiotic and metabolic pathways, while negatively affecting extracellular matrix formation and organization. A role of the neutrophils in the mechanisms underlying BaP effect on bone formation and regeneration through their interaction with bone extracellular matrix or bone forming cells, the osteoblasts, was also evidenced. This is not the first time that PAHs are associated with adverse effects on bone formation and regeneration. An impaired growth of the operculum was recently evidenced in larvae exposed to 3-methylcholanthrene (3-MC) (Laizé et al., 2018), another member of the PAH family, and effective concentrations for 3-MC are in the same range of those determined here for BaP, although a bit higher (from 3.7 to 117 μM). This comparable effect could be related to their close molecular structure, which differs only in 1 carbon and 4 hydrogen atoms. It is also worth mentioning that larvae exposed to concentrations higher than 10 μM displayed a decrease in total length and head area, thus BaP may also trigger a more general growth retardation at higher concentrations, besides a specific effect on bone. The BaP action on bone mineral density evidenced here in newly formed fin rays and scales was also described in the Japanese medaka (*Oryzias latipes*). It was shown that parental administration of BaP was able to inhibit centra mineralization in offspring larvae (F1-F3 generations), suggesting that BaP osteotoxicity can affect a large range of bone structures and also be inherited by next generations (Seemann et al., 2017; Mo et al., 2020). Delay in caudal vertebrae ossification was also reported during rat development following parental dietary exposure to BaP (da Silva Moreira et al., 2021). *In vitro* data collected from mammalian cell systems also evidenced that BaP can reduce mineral deposition in human periodontal ligament (HPDLC) and mesenchymal stem cells (C3H10T1/2, MEF, HCT116 and hBM-MSCs) (Monnouchi et al., 2016; An et al., 2020; Zhou et al., 2017), confirming not only the anti-mineralogenic effect of BaP, but also that mechanisms of action may be conserved throughout vertebrate evolution, from fish to human. The strong reduction of the fluorescence signal associated with *osteocalcin* expression, a marker of mature osteoblasts (Capulli et al., 2014), indicated that BaP osteotoxicity in the operculum may be related to an impairment of osteoblast differentiation. A reduction in *osteocalcin* expression was also confirmed by qPCR in BaP-treated zebrafish larvae (this study) and mesenchymal stem cell cultures (An et al., 2020). Osteocalcin is a bone matrix protein mainly produced by osteoblasts, which is involved in bone matrix formation and mineralization (Gavaia et al., 2006; Manolagas, 2020). Impaired osteoblast differentiation associated with a reduced number of mature osteoblasts and a reduced production of osteocalcin could be the basis for the reduced bone growth and mineralization observed upon BaP exposure. Interestingly, the fluorescence signal associated with *osterix* expression, a marker of immature osteoblasts (Sinha and Zhou, 2013), was not reduced upon larvae exposure to BaP – it was even slightly increased – while qPCR data showed no effect of BaP exposure on *osterix* expression (this study). The apparent absence of effect on immature osteoblast would indicate that BaP specifically targets late osteoblast maturation. On the contrary, BaP parental exposure reduced *col10* and *sp7* fluorescence signals in vertebrae of 26-dpf medaka from F1-F3 generations (Mo et al., 2020) and *sp7* expression in 17 days post-hatching (dph) medaka larvae from F2 and F3 generations (Seemann et al., 2015). These differences may be related to the different animal model (i.e., zebrafish vs medaka), type of exposure (i.e., direct vs parental), bone structure assessed (i.e., operculum vs vertebrae) and the different endpoint (i.e., 6 dpf vs. 17/26 dpf). It is important to mention that, while *sp7* expression was reduced in medaka F2 and F3 generations, it was not affected in medaka F1 generation, emphasizing the complexity of BaP effect on this marker gene. In this regard, the same two studies show that other markers of osteoblast proliferation, *runx2* and *bmp2*, were up-regulated upon BaP exposure (Seemann et al., 2015, 2017).

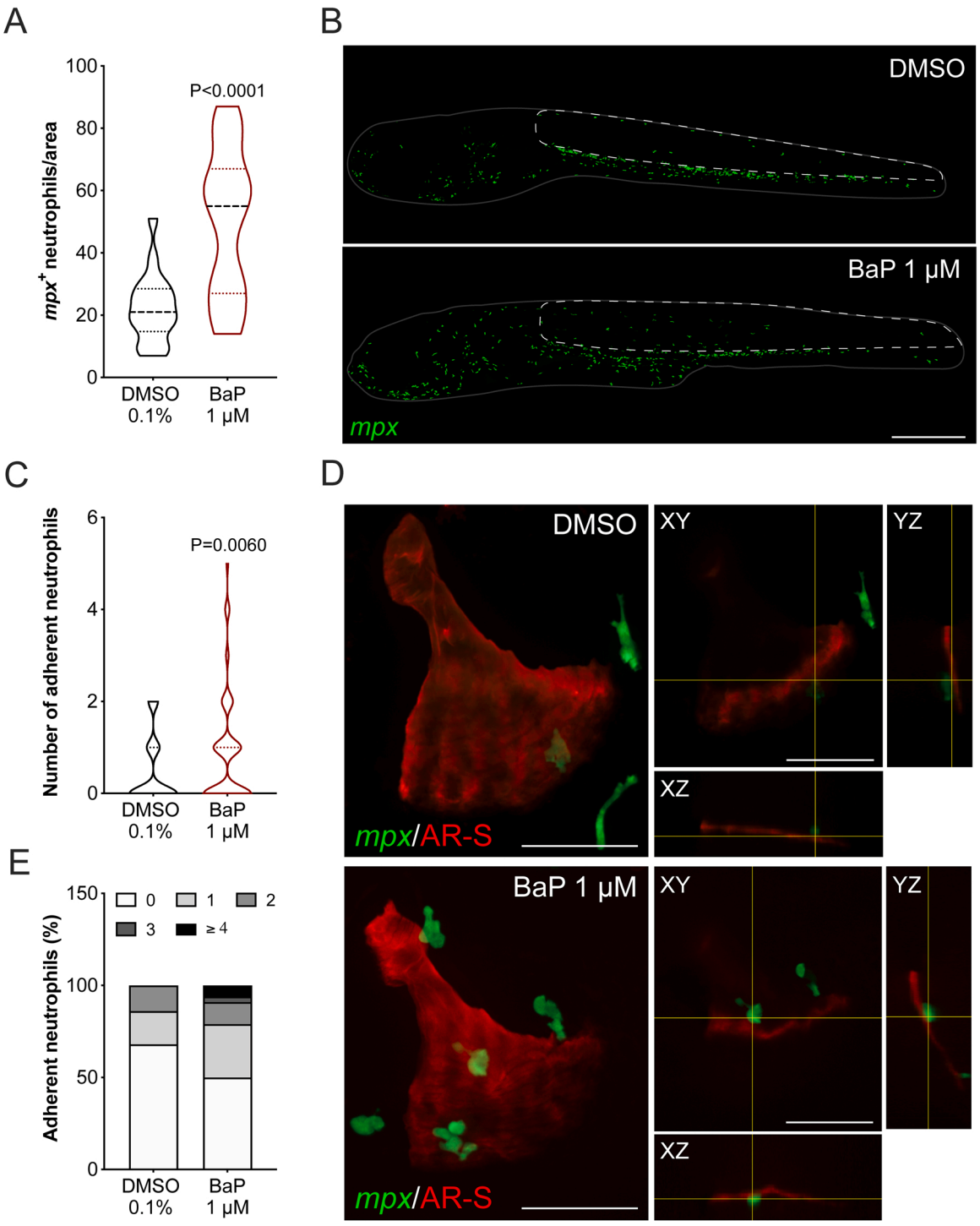

Fig. 7. Number of neutrophils in *TgBAC(mpx:EGFP)*^{i114} zebrafish larvae exposed to BaP from 3 to 6 dpf. (A) Number of neutrophils in the region of interest (ROI) expressed in % over control. (B) Representative images of transgenic larvae exposed to 0.1% DMSO or 1 µM BaP, where *TgBAC(mpx:EGFP)*^{i114} positive cells are in green. ROI is outlined with a white dashed line, while larvae is outlined with a gray line. Scale bar is 500 µm. P-value calculated using Student's *t*-test. Values are presented as median and quartiles (n = 18). (*C*) Number of adherent neutrophils on the opercular bone stained with AR-S. P-value calculated using Mann Whitney test. Values are presented as median and quartiles (n = 109). (D) Representative images of adherent neutrophils on the operculum of larvae exposed to 0.1% DMSO or 1 µM BaP, where *TgBAC(mpx:EGFP)*^{i114} positive cells are in green and operculum is in red. On the right side of the representative images, orthogonal projections of the planes (XY, YZ and XZ) marked with the yellow lines. Scale bar is 50 µm. (E) Percentage of adherent neutrophils at 6 dpf per opercular bone. Colors indicate the number of *TgBAC(mpx:EGFP)*^{i114} positive cells per operculum. For interpretation of the references to color in this figure legend, the reader is referred to the web version of this article.

Based on our experimental results, we propose that BaP osteotoxic effect on the operculum growth is the result of an inhibition of the final step of osteoblast maturation, which leads to a decrease in operculum growth and mineralization. The slight increase of immature osteoblasts in zebrafish larval operculum may be a feedback response to BaP osteotoxic effect or an accumulation of immature cells that failed to differentiate.

Few studies have reported the occurrence of skeletal anomalies upon BaP exposure. While no skeletal effects were observed in rat fetus after parental dietary exposure (da Silva Moreira et al., 2021), BaP triggered spinal curvatures and jaw defects in the false kelpfish *Sebastiscus marmoratus* after 7 days of waterborne exposure (He et al., 2011) and multigenerational bone deformities in medaka F1-F3 generations (Seemann et al., 2015, 2017) and zebrafish F1-F2 generations (Corrales et al., 2014) after parental dietary exposure. Our data collected in zebrafish juveniles exposed for 27 days to waterborne BaP further supports the skeletotoxic effect of BaP and revealed that 100% of the fish were deformed at the highest non-lethal concentration (1 μM). Most of the BaP concentrations found in the environment fall within the range of 6.3×10^{-7} to 4.5×10^{-5} μM (Suvarapu and Baek, 2017; Moon et al., 2007; Manoli and Samara, 1999) and are below the lowest effective concentration determined in this study, although much higher concentrations (i.e., 1.9×10^{-2} μM) have been reported (Zhou and Maskaoui, 2003)). Still, an exposure to sub-effective concentrations for periods longer that those reported here, a situation that may regularly occur in the environment, could lead to skeletal anomalies at concentrations lower than 0.01 μM.

It is important to mention that the incidence of deformities observed in the control group (50%) is within the normal range (45–65%) for wild-type zebrafish (Roberto et al., 2018; Martins et al., 2019). BaP exposure affected different skeletal structures, but no particular pattern was identified, except for the occurrence of anomalies in the head structures (e.g., opercular bones) in the higher concentrations tested. The most common anomalies were fusions of vertebrae and arches, deformed vertebrae and arches, cases of platyspondyly or ectopic mineralization. Our data also revealed that the regions of the axial skeleton mostly affected by BaP were the caudal vertebrae, caudal fin vertebrae and the caudal fin complex. These regions were also found to be more prone to deformities in other studies in zebrafish (Martins et al., 2019; Fazenda et al., 2018) and also in other fish species (Boglione et al., 2013), for reasons that remain to be better understood, but could be related to their central role in locomotion, their close position to the swimming bladder and other developmental factors (Bagwell et al., 2020; Martini et al., 2020; Bensimon-Brito et al., 2010). It is worth mentioning that several of the fish exposed to the highest concentrations of BaP also presented a deformed operculum. Therefore, BaP-exposed fish may develop deformities that could affect locomotion and fitness, thus reducing their ability to feed or avoid predation in the nature. Although this should be further investigated, an increase on the incidence of skeletal deformities upon BaP exposure may result from an unbalanced resorption and formation during bone remodeling process or alteration in extracellular matrix components and organization (Laizé et al., 2018; Witten and Hall, 2015; Boursiaki et al., 2019; Gray et al., 2021).

Scale regeneration in zebrafish is achieved through a succession of differentiation, proliferation, and parallel routes of shape change or cell death of the osteoblast (Cox et al., 2018). Our data showed smaller regenerated scales in fish exposed to BaP, which is consistent with a reduced bone formation by osteoblasts. It is also in agreement with published data showing that an exposure of *ex vivo* cultured zebrafish scales to 5 and 50 μM BaP (concentrations higher than those tested in this study) inhibited Sp7 activity, evidencing an effect on osteoblast differentiation that may be related to a reduced bone formation (Torvanger et al., 2018). Similarly, exposure of *ex vivo* cultured goldfish scales to seawater polluted with a mixture of PAHs (including BaP at concentrations ranging from 26 to 49 ng/L) showed that osteoblast activity and marker genes were strongly affected (Suzuki et al., 2016). Our data showing intense TRAP activity and regions of strong demineralization also indicated that BaP may stimulate osteoclast activity thus the resorption of the mineralized matrix. Data from literature is scarce and limited to *ex vivo* cultures of goldfish scales. While TRAP activity was unaltered in scales exposed to a mixture of PAHs (Suzuki et al., 2016), Mmp9 activity was decreased in scales exposed to BaP, suggesting reduced bone resorption (Torvanger et al., 2018). Discrepancy on the effect of BaP on osteoclast activity and bone resorption may be related to the species (i.e., zebrafish vs goldfish), exposure time (5 vs 2 days), and biological material (i.e., regenerating vs *ex vivo* scales) used in the different studies. Based on available data, we propose that BaP exerts its osteotoxic effect through a dual action on bone cells: an impaired osteoblast differentiation resulting in a reduced scale regeneration and an increased osteoclast activity resulting in an increased scale demineralization. The combined effect would result in an abnormal bone formation and remodeling leading to smaller and misshaped scales.

BaP was also found to affect caudal fin regeneration and *de novo* bone formation. As for scale, the size of the regenerated fin and the mineralization and shape of the newly formed bone were impaired, indicating that similar mechanisms may be involved. Other toxicants have been previously shown to affect zebrafish caudal fin regeneration. TCDD inhibited caudal fin tissue regeneration in larvae at 5 dpf (Mathew et al., 2006) (exposed for 3 days after amputation at 2 dpf) and in adult up to 21 dpa (Zodrow and Tanguay, 2003), while 3-MC not only affected tissue regeneration in adults regenerating their caudal fin but also impaired calcification (Laizé et al., 2018). However, previous studies did not evaluate the effects of PAHs on regeneration of caudal fin rays, patterning and total mineralization area. Although the mineralized bone area of the caudal fin was not affected upon BaP exposure at all concentrations tested, analysis of μCT images revealed that the mineral density of the rays was affected from the amputation plane throughout the ray. This could be related to impaired osteoblast differentiation and/or deposition of matrix mineral. Shaping of the caudal fin rays was also affected at all concentrations tested, resulting in a proximalization of the point of the first bifurcation. Although the mechanisms of ray bifurcation during development or regeneration are not fully understood, recent studies have shown that ray branching may be controlled by either Shh/Smo (Sonic hedgehog/Smoothened) signaling (Braunstein et al., 2021), levels of thyroid hormone (Hu et al., 2020) and even water temperature (Christou et al., 2018). Interestingly, hyperthyroid fish display a proximalization of the bifurcation points. In this regard, BaP is a known endocrine disruptor and several studies have shown that an exposure to BaP increases levels of thyroid hormone in rat hepatocytes (Schraplau et al., 2015) and of thyroid stimulating hormone (TSH) in Abu mullet (Movahedinia et al., 2018). Although this should be further tested, BaP effect on ray bifurcation could be related to its action on thyroid hormone homeostasis. It will be also interesting to evaluate, in future studies, which genes are involved in ray patterning plasticity that may be affected by external stressors such as temperature or contaminants (BaP in the case of this study).

The lesser extent of fin regeneration in fish exposed to BaP may result from an inhibition of the pathways involved in fin regenerative outgrowth (as also suggested for TCDD (Zodrow and Tanguay, 2003)), a hypothesis that we did not explore in this work. Although not quantified, an hyperpigmentation was observed in regenerated fin exposed to BaP, indicating that BaP may stimulate melanocytes differentiation or proliferation, possibly through the activation of the AHR receptor as reported for TCDD (Zodrow and Tanguay, 2003) and ambient particulate matter, which is known to absorb many PAHs and metals (Peng et al., 2019).

To gain insights into the mechanisms of BaP osteotoxicity, transcriptomic data was collected from larvae exposed to DMSO or BaP for 3 days. Pathway enrichment of differentially expressed genes confirmed the role of xenobiotic related pathways such as phase I functionalization

of compounds, phase II conjugation of compounds, glutathione conjugation, metabolism and biological oxidation, in particular the marker genes *ahr2*, *nr1i2*, *cyp1a* and *gstp1*, all up-regulated upon BaP exposure. A similar trend was reported in several *in vitro* and *in vivo* systems upon exposure to BaP but also to other PAHs. AHR and NR1I2 are xenobiotic-dependent transcription factors involved in the regulation of phase I and phase II metabolizing enzymes, which detoxify harmful compounds in order to protect the organisms. An up-regulation of these genes was also observed in zebrafish exposed to 3-MC, although to a lower extent, probably due to the different concentrations tested (Laizé et al., 2018). Besides mediating xenobiotic toxic effects, AHR has been shown to regulate several physiological and pathological processes (e.g., hematopoiesis, inflammation, immune response, detoxification and cancer) and of interest to this study, bone metabolism (Stockinger et al., 2014; Larigot et al., 2018). AHR is in fact expressed in osteoblastic and osteoclastic cells and it also plays a role in ECM homeostasis (Roztocil et al., 2020; Park et al., 2020; Yu et al., 2018). In this work, *ahr2* expression was assessed globally and it is therefore not possible to associate its upregulation to any specific process.

Pathways related to extracellular matrix degradation, formation and organization (e.g., collagen chain trimerization, collagen synthesis, formation and degradation, ECM degradation and formation, activation of metalloproteinases) were also enriched in BaP-treated larvae. In this regard, the altered expression of bone marker genes (i.e., *oc2*, *col1a1a*, *col2a1a*, *col10a1a* and *spp1*) coding for extracellular matrix proteins involved in bone formation and mineralization is consistent with impaired osteoblast differentiation and reduced bone formation observed in BaP-treated larvae.

As observed in zebrafish exposed to 3-MC (Laizé et al., 2018), BaP exposure induced, albeit only slightly, the expression of *vdrb* and *alpl*. In mammals and fish, vitamin D receptor (VDR) and alkaline phosphatase (ALP) are central to osteoblast function, activity and bone formation (Zarei et al., 2016; van de Peppel et al., 2018; Vimalraj, 2020), and their increased expression in BaP-treated larvae may not fit the osteotoxic effect observed here. An increase of *vdrb* could however be related to its role in xenobiotic response since, in fact, VDR transactivation can be a target for several xenobiotics (such as 7-methylbenzo[α]pyrene) (Mahapatra et al., 2018) and induce the transcription of metabolizing enzymes (Baldwin, 2019; Qin and Wang, 2019). In this regard, induction of CYP1A expression by VDR activation was only reported in human monocyte/macrophage-derived cells to respond to BaP-mediated toxicity (Matsunawa et al., 2009, 2012). Increased expression of *alpl* is probably related to liver damage as reported in fish exposed to other PAH (Haque et al., 2017).

The molecular mechanisms underlying the activation of osteoclast differentiation by BaP have never been reported in fish. In mouse *in vitro* system, BaP stimulated osteoclastogenesis through the activation of AhR and the involvement of a RANKL/AhR/c-Fos signaling axis (Izawa et al., 2016, 2017). Our expression data is consistent with this mechanism, with genes involved in osteoclast differentiation (*fosab*, *ctsk*) and activity (*acp5a/b* and *mmp9/13*) up regulated in BaP-treated larvae. Thus, the role of AHR/c-Fos signaling pathway in the stimulation of osteoclast activity by BaP may have been conserved throughout vertebrate evolution.

Finally, transcriptomic analysis showed a 2-fold enrichment in genes related to neutrophil degranulation. At the beginning of an acute inflammation that may result from a bacterial infection, cancers and exposure to environmental pollutants, neutrophils migrate to site of inflammation, where they release factors such as chemokine/cytokines to help other cell respond with a proper immune response, or undergo degranulation (Mollinedo, 2019; Havixbeck et al., 2016; Havixbeck and Barreda, 2015). During degranulation, proteins such as myeloperoxidase, elastase, gelatinase and collagenase present in the granules are released into the extracellular environment. Excessive neutrophil degranulation has been described in many inflammatory disorders, such as lung injury (Yang et al., 2020), severe asthma (Ray and Kolls, 2017) and rheumatoid arthritis (Wright et al., 2010). Several *in vitro/in vivo* studies in mammalian and fish systems have shown that exposure to BaP can trigger an inflammatory response (Shi et al., 2017; Barnwal et al., 2018; Xie et al., 2020; Rehberger et al., 2021), a situation confirmed here with the increased expression of well-established inflammatory markers such as *il-6* and *il-1β* in BaP-treated larvae. Our data also indicate that the number of neutrophils increased upon BaP exposure in the whole-larvae and in the fish trunk. Again, expression data further supported BaP effect on neutrophils, as neutrophil marker genes such as *mpx*, *lyz* and *mmp9* were up regulated in BaP-treated larvae. Further studies should determine whether neutrophil activation results from BaP-induced inflammation or AHR activation in fish. Several studies in mammalian models have shown that AHR signaling stimulates neutrophils recruitment (Hao and Whitelaw, 2013; Hanieh, 2014) and, recently, that Ahr is functional in teleost (e.g., rainbow trout) immune cells (Song et al., 2020). An interaction between neutrophils and the opercular bone was observed in our study. Interestingly, the number of interacting neutrophils increased in fish exposed to BaP. This is to the best of our knowledge, the first evidence (in fish and in any *in vivo* model) that neutrophils may interact directly with bone structures. Whether they interact with osteoblasts or ECM remains to be established in our system, but *in vitro* studies can already give us some hints. Allaeys et al. (2011) showed that exposure of human osteoblast (grown from trabecular bone explants) to monosodium urate (crystal deposited in chronic gut disease) promoted neutrophils adherence to osteoblast. It has also been suggested that neutrophils induced osteoblast retraction leaving the ECM more vulnerable to active osteoclast, a process that leads to an imbalanced bone formation/resorption. A more recent study by Bastian et al. (2018) showed that neutrophils inhibited the synthesis of ECM mineralization by human bone marrow stromal cells (BMSCs). These authors also showed that co-culture of BMSCs with neutrophils induced a decrease in cell density and both ALP activity and ECM mineralization were significantly reduced. A stimulation of osteoclast differentiation by neutrophils was also reported in mice, both *in vivo* and *in vitro*. In this regard, Kim et al. (2020) showed in a mouse periodontitis and air pouch model, that the presence of neutrophils could induce RANKL expression in periodontal tissue and stimulate osteoclast formation. Sugisaki et al. (2020) showed that human neutrophils enhanced osteoclast differentiation in co-cultures of mouse bone marrow cells and osteoblasts. We propose that neutrophils play a major role in BaP osteotoxicity through a mechanism that probably involves an initial inflammatory event induced by BaP, a recruitment of neutrophils following inflammation and an increased interaction of neutrophils with bone structures, resulting in less bone formed or more bone lost. A simple scheme of the molecular mechanisms of BaP osteotoxicity in zebrafish is presented in Fig. 8, where the activation of AHR and PXR signaling pathways regulates not only the expression of xenobiotic metabolizing enzymes but also genes involved in the differentiation and function of bone forming and resorbing cells and neutrophils.

5. Conclusions

This study demonstrated the strong osteotoxic effects of BaP throughout zebrafish development and regeneration. By inhibiting osteoblast maturation and ECM mineralization and stimulating osteoclast activity, BaP impacted both bone formation and resorption, thus bone remodeling. Consequences of BaP on bone remodeling were seen both after a long exposure (27 days) in developing larvae, i.e., an increased incidence and severity of skeletal deformities in the axial skeleton, and after a short exposure (5 days) in regenerating adults, leading to misshaped and demineralized newly formed fin rays and scales. Transgenic and transcriptomic approaches helped us to gain insights into cellular and molecular mechanisms underlying BaP osteotoxicity. We believe that, besides the activation of xenobiotic and metabolic pathways through Ahr2 and/or Pxr, which may negatively impact extracellular matrix formation and organization, BaP activates

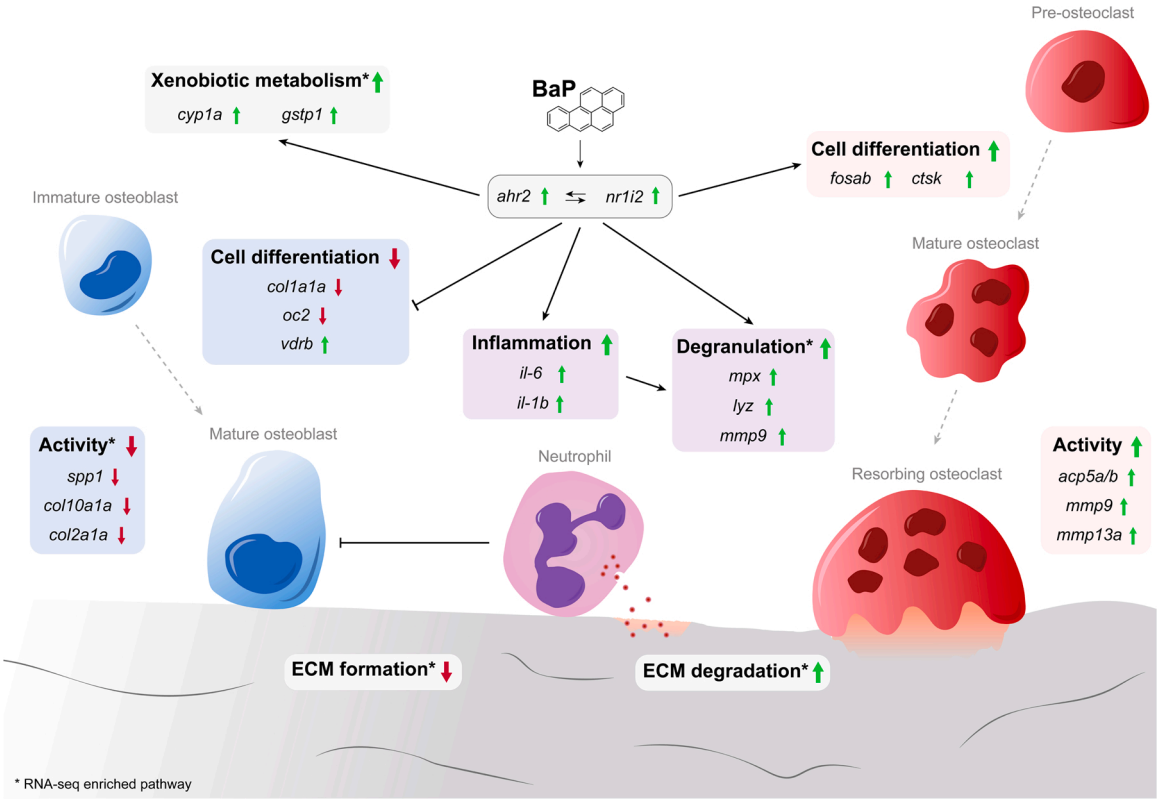

Fig. 8. Schematic overview of the possible mechanisms underlying the BaP osteotoxicity in zebrafish larvae. Vertical arrows after gene names indicate increased (upward pointing green arrow) and decreased (downward pointing red arrow) gene expression. Asterisks indicate enriched pathways supported by RNA-seq. For interpretation of the references to color in this figure legend, the reader is referred to the web version of this article.

inflammatory mechanisms that recruit neutrophils, which affect both osteoblast and osteoclast activity, possibly through a direct interaction of the neutrophils with the bone matrix. Future studies should aim at further exploring the crosstalk mechanisms between immune system and bone, in particular characterizing the role of neutrophils in bone homeostasis. In a more global context, it would be of utmost interest to investigate whether pollutants of the PAH family, especially those with 2 or 3 rings (e.g., naphthalene and anthracene) or those with a more complex structure, have a similar effect on fish bone.

Disclosure

The authors declare that they do not have any conflict of interest. The data that support the findings of this study are available from the corresponding author upon reasonable request.

CRediT authorship contribution Statement

Marco Tarasco: Conceptualization, Investigation, Methodology, Validation, Visualization, Writing – original draft, Writing – review & editing. **Paulo J. Gavaia:** Conceptualization, Investigation, Methodology, Validation, Writing – review & editing, Writing – funding acquisition. **Anabela Bensimon-Brito:** Conceptualization, Investigation, Methodology, Validation, Writing – review & editing. **João Cardeira da Silva:** Conceptualization, Methodology, Validation, Writing – review & editing. **Srinath Ramkumar:** Investigation, Writing – review & editing. **Fabrice Cordelières:** Methodology, Resources, Software, Writing – review & editing. **Stefan Günther:** Resources, Software. **Maria J. Bebianno:** Supervision, Writing – review & editing. **Didier Y. R. Stainier:** Resources, Supervision, Writing – review & editing, Funding acquisition. **M. Leonor Cancela:** Resources, Supervision, Writing – review & editing, Funding acquisition. **Vincent Laizé:** Conceptualization, Methodology, Resources, Supervision, Validation, Visualization, Writing – review & editing, Funding acquisition.

Declaration of Competing Interest

The authors declare that they have no known competing financial interests or personal relationships that could have appeared to influence the work reported in this paper.

Acknowledgments

We thank Stefan Schulte-Merker for providing *Tg(Ola.Sp7:mCherry-Eco.NfsB)*^{pd46} and *Tg(Ola.osteocalcin:EGFP)*^{hu4008} zebrafish lines and Steve Renshaw for providing *TgBAC(mpx:GFP)*^{i114} zebrafish line. This study was funded by Portuguese national funds from the Foundation for Science and Technology (FCT) through projects UIDB/04326/2020 and UID/00350/2020, and by the European Maritime and Fisheries Fund (EMFF/FEAMP) through the National Operational Program MAR2020 and project OSTEOMAR MAR-02.01.01-FEAMP-0057. Marco Tarasco was supported by the FCT through the PhD grant SFRH/BD/128634/2017 and by NEUBIAS-COST STSM program as part of action CA15124. The Bordeaux Imaging Center is a member of the national infrastructure France BioImaging supported by the French National Research Agency (ANR-10-INBS-04).

Appendix A. Supporting information

Supplementary data associated with this article can be found in the online version at doi:10.1016/j.ecoenv.2021.112838.

References

Al-Bashaireh, A.M., Haddad, L.G., Weaver, M., Chengguo, X., Kelly, D.L., Yoon, S., 2018. The effect of tobacco smoking on bone mass: an overview of pathophysiologic mechanisms. J. Osteoporos. 2018, 1–17.

Allaeys, I., Rusu, D., Picard, S., Pouliot, M., Borgeat, P., Poubelle, P.E., 2011. Osteoblast retraction induced by adherent neutrophils promotes osteoclast bone resorption: implication for altered bone remodeling in chronic gout. Lab Invest. 91 (6), 905–920.

An, L., Shi, Q., Fan, M., Huang, G., Zhu, M., Zhang, M., Liu, Y., Weng, Y., 2020. Benzo[a] pyrene injures BMP2-induced osteogenic differentiation of mesenchymal stem cells through AhR reducing BMPRII. Ecotoxicol. Environ. Saf. 203, 110930.

Andrews S.(2010). FastQC: A Quality Control Tool for High Throughput Sequence Data. (http://www.bioinformatics.babraham.ac.uk/projects/fastqc/).

Bagwell, J., Norman, J., Ellis, K., Peskin, B., Hwang, J., Ge, X., Nguyen, S.V., McMenamin, S.K., Stainier, D.Y., Bagnat, M., 2020. Notochord vacuoles absorb compressive bone growth during zebrafish spine formation. Elife 9, 1–28.

Baldwin, W.S., 2019. Phase 0 of the xenobiotic response: nuclear receptors and other transcription factors as a first step in protection from xenobiotics. Nucl. Recept Res. 6.

Barnwal, P., Vafa, A., Afzal, S.M., Shahid, A., Hasan, S.K., Sultana, S., Alpashree, 2018. Benzo(a)pyrene induces lung toxicity and inflammation in mice: prevention by carvacrol. Hum. Exp. Toxicol. 37 (7), 752–761.

Barron, M.G., Carls, M.G., Heintz, R., Rice, S.D., 2004. Evaluation of fish early life-stage toxicity models of chronic embryonic exposures to complex polycyclic aromatic hydrocarbon mixtures. Toxicol. Sci. 78 (1), 60–67.

Bastian, O.W., Croes, M., Alblas, J., Koenderman, L., Leenen, L.P.H., Blokhuis, T.J., 2018. Neutrophils inhibit synthesis of mineralized extracellular matrix by human bone marrow-derived stromal cells *in vitro*. Front Immunol. 9, 945.

Bensimon-Brito, A., Cancela, M.L., Huysseune, A., Witten, P.E., 2010. The zebrafish (Danio rerio) caudal complex – a model to study vertebral body fusion. J. Appl. Ichthyol. 26 (2), 235–238.

Bensimon-Brito, A., Cardeira, J., Dionísio, G., Huysseune, A., Cancela, M.L., Witten, P.E., 2016. Revisiting *in vivo* staining with alizarin red S – a valuable approach to analyse zebrafish skeletal mineralization during development and regeneration. BMC Dev. Biol. 16 (1), 1–10.

Bird, N.C., Mabee, P.M., 2003. Developmental morphology of the axial skeleton of the zebrafish,Danio rerio (Ostariophysi: Cyprinidae). Dev. Dyn. 228 (3), 337–357.

Boglione, C., Gisbert, E., Gavaia, P., E. Witten, P., Moren, M., Fontagné, S., Koumoundouros, G., 2013. Skeletal anomalies in reared European fish larvae and juveniles. Part 2: main typologies, occurrences and causative factors. Rev. Aquac. 5 (Suppl.1), 121–167.

Bolger, A.M., Lohse, M., Usadel, B., 2014. Trimmomatic: a flexible trimmer for Illumina sequence data. Bioinformatics 30 (15), 2114–2120.

Boursiaki, V., Theochari, C., Zaoutsos, S., Mente, E., Vafidis, D., Apostologamvrou, C., Berillis, P., 2019. Skeletal deformity of scoliosis in gilthead seabreams (Sparus aurata): association with changes to calcium-phosphor hydroxyapatite salts and collagen fibers. Water 11 (2), 257.

Braunstein, J.A., Robbins, A.E., Stewart, S., Stankunas, K., 2021. Basal epidermis collective migration and local Sonic hedgehog signaling promote skeletal branching morphogenesis in zebrafish fins. bioRxiv 55 (2), 312–317.

Capulli, M., Paone, R., Rucci, N., 2014. Osteoblast and osteocyte: games without frontiers. Arch. Biochem. Biophys. 561, 3–12.

Cardeira, J., Gavaia, P.J., Fernández, I., Cengiz, I.F., Moreira-Silva, J., Oliveira, J.M., Reis, R.L., Cancela, M.L., Laizé, V., 2016. Quantitative assessment of the regenerative and mineralogenic performances of the zebrafish caudal fin. Sci. Rep. 6, 39191.

Carls, M.G., Thedinga, J.F., 2010. Exposure of pink salmon embryos to dissolved polynuclear aromatic hydrocarbons delays development, prolonging vulnerability to mechanical damage. Mar. Environ. Res. 69 (5), 318–325.

Chen, Y.Y., Kao, T.W., Wang, C.C., Wu, C.J., Zhou, Y.C., Chen, W.L., 2020. Association between polycyclic aromatic hydrocarbons exposure and bone turnover in adults. Eur. J. Endocrinol. 182 (3), 333–341.

Christou, M., Iliopoulou, M., Witten, P.E., Koumoundouros, G., 2018. Segmentation pattern of zebrafish caudal fin is affected by developmental temperature and defined by multiple fusions between segments. J. Exp. Zool. Part B Mol. Dev. Evol. 1–11.

Collier, T.K., Anulacion, B.F., Arkoosh, M.R., Dietrich, J.P., Incardona, J.P., Johnson, L. L., Ylitalo, G.M., Myers, M.S., 2013. Effects on fish of polycyclic aromatic hydrocarbonS (PAHS) and naphthenic acid exposures. Fish. Physiol. 33, 195–255.

Corrales, J., Thornton, C., White, M., Willett, K.L., 2014. Multigenerational effects of benzo[a]pyrene exposure on survival and developmental deformities in zebrafish larvae. Aquat. Toxicol. 148, 16–26.

Cox, B.D., De Simone, A., Tornini, V.A., Singh, S.P., Di Talia, S., Poss, K.D., 2018. In Toto imaging of dynamic osteoblast behaviors in regenerating skeletal bone. Curr. Biol. 28 (24), 3937–3947 e4.

da Silva Moreira, S., de Lima Inocêncio, L.C., Jorge, B.C., Reis, A.C.C., Hisano, H., Arena, A.C., 2021. Effects of benzo(a)pyrene at environmentally relevant doses on embryo-fetal development in rats. Environ. Toxicol. 36 (5).

Danion, M., Deschamps, M.H., Thomas-Guyon, H., Bado-Nilles, A., Le Floch, S., Quentel, C., Sire, J.Y., 2011. Effect of an experimental oil spill on vertebral bone tissue quality in European sea bass (Dicentrarchus labrax L.). Ecotoxicol. Environ. Saf. 74 (7), 1888–1895.

De Gelder, S., Bakke, M.J., Vos, J., Rasinger, J.D., Ingebrigtsen, K., Grung, M., Ruus, A., Flik, G., Klaren, P.H.M., Berntssen, M.H.G., 2016. The effect of dietary lipid composition on the intestinal uptake and tissue distribution of benzo[a]pyrene and phenanthrene in Atlantic salmon (Salmo salar). Comp. Biochem. Physiol. Part - C. Toxicol. Pharm. 185, 65–76.

Dobin, A., Davis, C.A., Schlesinger, F., Drenkow, J., Zaleski, C., Jha, S., Batut, P., Chaisson, M., Gingeras, T.R., 2013. STAR: ultrafast universal RNA-seq aligner. Bioinformatics 29 (1), 15–21.

Fazenda, C., Martins, G., Gavaia, P.J., Cancela, M.L., Conceição, N., 2018. Generation of zebrafish Danio rerio (Hamilton, 1822) transgenic lines overexpressing a heat-shock mediated Gla-rich protein. J. Appl. Ichthyol. 34 (2), 472–480.

Fernández, I., Gavaia, P.J., Laizé, V., Cancela, M.L., 2018. Fish as a model to assess chemical toxicity in bone. Aquat. Toxicol. 194, 208–226.

Gavaia, P.J., Simes, D.C., Ortiz-Delgado, J.B., Viegas, C.S., Pinto, J.P., Kelsh, R.N., Sarasquete, M.C., Cancela, M.L., 2006. Osteocalcin and matrix Gla protein in zebrafish (Danio rerio) and Senegal sole (Solea senegalensis): comparative gene and protein expression during larval development through adulthood. Gene Expr. Patterns 6 (6), 637–652.

Gray, R.S., Gonzalez, R., Ackerman, S.D., Minowa, R., Griest, J.F., Bayrak, M.N., Troutwine, B., Canter, S., Monk, K.R., Sepich, D.S., Solnica-Krezel, L., 2021. Postembryonic screen for mutations affecting spine development in zebrafish. Dev. Biol. 471, 18–33.

Guo, J., Huang, Y., Bian, S., Zhao, C., Jin, Y., Yu, D., Wu, X., Zhang, D., Cao, W., Jing, F., Chen, G., 2018. Associations of urinary polycyclic aromatic hydrocarbons with bone mass density and osteoporosis in U.S. adults, NHANES 2005–2010. Environ. Pollut. 240, 209–218.

Hadrup, N., Mielzyńska-Švach, D., Kozłowska, A., Campisi, M., Pavanello, S., Vogel, U., 2019. Association between a urinary biomarker for exposure to PAH and blood level of the acute phase protein serum amyloid A in coke oven workers. Environ. Health A Glob. Access Sci. Source 18 (1), 1–9.

Hall, B.K., 2015. Bones and Cartilage [Internet]. Elsevier.

Hanieh, H., 2014. Toward understanding the role of aryl hydrocarbon receptor in the immune system: current progress and future trends. Biomed. Res. Int. 2014, 520763.

Hao, N., Whitelaw, M.L., 2013. The emerging roles of AhR in physiology and immunity. Biochem. Pharm. 86 (5), 561–570.

Haque, S., Mondal, S., Kundu, D., Ghosh, A.R., 2017. Effect of multiple polycyclic aromatic hydrocarbons (Pahs) on liver of three teleostean fishes Labeobata, Labeorohita and Cirrhinusmrigala in Burdwan Loco Tank, Burdwan, West Bengal, India. Austin Environ. Sci. 2 (1), 1–8.

Havixbeck, J., Barreda, D., 2015. Neutrophil development, migration, and function in teleost fish. Biology 4 (4), 715–734.

Havixbeck, J.J., Rieger, A.M., Wong, M.E., Hodgkinson, J.W., Barreda, D.R., 2016. Neutrophil contributions to the induction and regulation of the acute inflammatory response in teleost fish. J. Leukoc. Biol. 99 (2), 241–252.

He, C., Zuo, Z., Shi, X., Li, R., Chen, D., Huang, X., Chen, Y., Wang, C., 2011. Effects of benzo (a) pyrene on the skeletal development of Sebastiscus marmoratus embryos and the molecular mechanism involved. Aquat. Toxicol. 101 (2), 335–341.

Hilton, D.C., Trinidad, D.A., Hubbard, K., Li, Z., Sjödin, A., 2017. Measurement of urinary Benzo[a]pyrene tetrols and their relationship to other polycyclic aromatic hydrocarbon metabolites and cotinine in humans. Chemosphere 189 (1), 365–372.

Hu, Y., Harper, M., Acosta, B., Donahue, J., Bui, H., Lee, H., Nguyen, S., McMenamin, S., 2020H. Thyroid hormone regulates proximodistal identity in the fin skeleton. bioRxiv.

Iqbal, J., Sun, L., Cao, J., Yuen, T., Lu, P., Bab, I., Leu, N.A., Srinivasan, S., Wagage, S., Hunter, C.A., Nebert, D.W., Zaidi, M., Avadhani, N.G., 2013. Smoke carcinogens cause bone loss through the aryl hydrocarbon receptor and induction of Cyp1 enzymes. Proc. Natl. Acad. Sci. 110 (27), 11115–11120.

Izawa, T., Arakaki, R., Mori, H., Tsunematsu, T., Kudo, Y., Tanaka, E., Ishimaru, N., 2016. The nuclear receptor AhR controls bone homeostasis by regulating osteoclast differentiation via the RANK/c-Fos signaling axis. J. Immunol. 197 (12), 4639–4650.

Izawa, T., Arakaki, R., Ishimaru, N., 2017. Crosstalk between cytokine RANKL and AhR signalling in osteoclasts controls bone homeostasis. J. Cytokine Biol. 2 (2).

Kim, A.R., Kim, J.H., Choi, Y.H., Jeon, Y.E., Cha, J.H., Bak, E.J., Yoo, Y.J., 2020. The presence of neutrophils causes RANKL expression in periodontal tissue, giving rise to osteoclast formation. J. Periodontal Res. 55 (6), 868–876.

Knopf, F., Hammond, C., Chekuru, A., Kurth, T., Hans, S., Weber, C.W., Mahatma, G., Fisher, S., Brand, M., Schulte-Merker, S., Weidinger, G., 2011. Bone regenerates via dedifferentiation of osteoblasts in the zebrafish fin. Dev. Cell 20 (5), 713–724.

Laizé, V., Gavaia, P.J., Cancela, M.L., 2014. Fish: a suitable system to model human bone disorders and discover drugs with osteogenic or osteotoxic activities. Drug Discov. Today Dis. Model. 13, 29–37.

Laizé, V., Gavaia, P.J., Tarasco, M., Viegas, M.N., Caria, J., Luis, N., Cancela, M.L., 2018. Osteotoxicity of 3-methylcholanthrene in fish. Ecotoxicol. Environ. Saf. 161, 721–728.

Lamichhane, S., Bal Krishna, K.C., Sarukkalige, R., 2016. Polycyclic aromatic hydrocarbons (PAHs) removal by sorption: a review. Chemosphere 148, 336–353.

Larigot, L., Juricek, L., Dairou, J., Coumoul, X., 2018. AhR signaling pathways and regulatory functions. Biochim. Open 7, 1–9.

Liao, Y., Smyth, G.K., Shi, W., 2014. FeatureCounts: an efficient general purpose program for assigning sequence reads to genomic features. Bioinformatics 30 (7), 923–930.

Mahapatra, D., Franzosa, J.A., Roell, K., Kuenemann, M.A., Houck, K.A., Reif, D.M., Fourches, D., Kullman, S.W., 2018. Confirmation of high-throughput screening data and novel mechanistic insights into VDR-xenobiotic interactions by orthogonal assays. Sci. Rep. 8 (1), 1–16.

Manolagas, S.C., 2020. Osteocalcin promotes bone mineralization but is not a hormone. PLoS Genet. 16 (6), 4–7.

Manoli, E., Samara, C., 1999. Polycyclic aromatic hydrocarbons in natural waters: sources, occurrence and analysis. Trends Anal. Chem. 18 (6), 417–428.

Martini, A., Huysseune, A., Witten, P.E., Boglione, C., 2021. Plasticity of the skeleton and skeletal deformities in zebrafish (Danio rerio) linked to rearing density. J. Fish. Biol. 98 (4), 971–986.
Martins, G., Diogo, P., Pinto, W., Gavaia, P.J., 2019. Early transition to microdiets improves growth, reproductive performance and reduces skeletal anomalies in zebrafish (Danio rerio). Zebrafish 16 (3), 300–307.
Mathew, L.K., Andreasen, E.A., Tanguay, R.L., 2006. Aryl hydrocarbon receptor activation inhibits regenerative growth. Mol. Pharm. 69 (1), 257–265.
Matsunawa, M., Amano, Y., Endo, K., Uno, S., Sakaki, T., Yamada, S., Makishima, M., 2009. The aryl hydrocarbon receptor activator benzo[a]pyrene enhances vitamin D3 catabolism in macrophages. Toxicol. Sci. 109 (1), 50–58.
Matsunawa, M., Akagi, D., Uno, S., Endo-Umeda, K., Yamada, S., Ikeda, K., Makishima, M., 2012. Vitamin D receptor activation enhances benzo[a]pyrene metabolism via CYP1A1 expression in macrophages. Drug Metab. Dispos. 40 (11), 2059–2066.
Mo, J., Au, D.W., Wan, M.T., Shi, J., Zhang, G., Winkler, C., Kong, R.Y., Seemann, F., 2020. Multigenerational impacts of benzo[a]pyrene on bone modeling and remodeling in Medaka (Oryzias latipes). Environ. Sci. Technol. 54 (19), 12271–12284.
Mollinedo, F., 2019. Neutrophil degranulation, plasticity, and cancer metastasis. Trends Immunol. 40 (3), 228–242.
Monnouchi, S., Maeda, H., Yuda, A., Serita, S., Wada, N., Tomokiyo, A., Akamine, A., 2016. Benzo[a]pyrene/aryl hydrocarbon receptor signaling inhibits osteoblastic differentiation and collagen synthesis of human periodontal ligament cells. J. Periodontal Res. 51 (6), 779–788.
Moon, H., Kang, S., Kim, H., Choi, M., Yu, J., Choi, H., et al., 2007. Polycyclic aromatic hydrocarbons (PAHs) in seawater and marine sediments from Mokpo Coast in Korea. J. Korean Soc. Environ. Anal. 10 (2), 83–90.
Movahedinia, A., Salamat, N., Kheradmand, P., 2018. Effects of the environmental endocrine disrupting compound benzo[a]pyrene on thyroidal status of abu mullet (Liza abu) during short-term exposure. Toxicol. Rep. 5, 377–382.
Oliveira, M., Capelas, S., Delerue-Matos, C., Morais, S., 2021. Grill workers exposure to polycyclic aromatic hydrocarbons: levels and excretion profiles of the urinary biomarkers. Int. J. Environ. Res. Public Health 18 (1), 1–15.
Olsvik, P.A., Hansen, B.H., Nordtug, T., Moren, M., Holen, E., Lie, K.K., 2011. Transcriptional evidence for low contribution of oil droplets to acute toxicity from dispersed oil in first feeding Atlantic cod (Gadus morhua) larvae. Comp. Biochem. Physiol. C. Toxicol. Pharm. 154 (4), 333–345.
Park, R., Madhavaram, S., Ji, J.D., 2020. The role of aryl-hydrocarbon receptor (AhR) in osteoclast differentiation and function. Cells 9 (10), 2294.
Peng, F., Tsuji, G., Zhang, J., Chen, Z., Furue, M., 2019. Potential role of PM2.5 in melanogenesis. Environ. Int. 132, 105063.
Pfaffl, M.W., 2001. A new mathematical model for relative quantification in real-time RT-PCR. Nucleic Acids Res. 29 (9), 45, 2001.
Qin, X., Wang, X., 2019. Role of vitamin D receptor in the regulation of CYP3A gene expression. Acta Pharm. Sin. B 9 (6), 1087–1098.
Ray, A., Kolls, J.K., 2017. Neutrophilic inflammation in asthma and association with disease severity. Trends Immunol. 38 (12), 942–954.
Rehberger, K., Escher, B.I., Scheidegger, A., Werner, I., Segner, H., 2021. Evaluation of an *in vitro* assay to screen for the immunotoxic potential of chemicals to fish. Sci. Rep. 11 (1), 1–16.
Renshaw, S.A., Loynes, C.A., Trushell, D.M.I., Elworthy, S., Ingham, P.W., Whyte, M.K.B., 2006. Atransgenic zebrafish model of neutrophilic inflammation. Blood 108 (13), 3976–3978.
Roberto, V.P., Martins, G., Pereira, A., Rodrigues, S., Grenha, A., Pinto, W., Cancela, M. L., Dias, J., Gavaia, P.J., 2018. Insights from dietary supplementation with zinc and strontium on the skeleton of zebrafish, Danio rerio (Hamilton, 1822) larvae: from morphological analysis to osteogenic markers. J. Appl. Ichthyol. 34 (2), 512–523.
Rondelli, C.M., Larsen, M.C., N'Jai, A., Czuprynski, C.J., Jefcoate, C.R., 2016. PAHs target hematopoietic linages in bone marrow through cyp1b1 primarily in mesenchymal stromal cells but not AhR: a reconstituted *in vitro* model. Stem Cells Int. 2016, 1–12.
Roztocil, E., Hammond, C.L., Gonzalez, M.O., Feldon, S.E., Woeller, C.F., 2020. The aryl hydrocarbon receptor pathway controls matrix metalloproteinase-1 and collagen levels in human orbital fibroblasts. Sci. Rep. 10 (1), 1–16.
Santonicola, S., De Felice, A., Cobellis, L., Passariello, N., Peluso, A., Murru, N., Ferrante, M.C., Mercogliano, R., 2017. Comparative study on the occurrence of polycyclic aromatic hydrocarbons in breast milk and infant formula and risk assessment. Chemosphere 175, 383–390.
Schraplau, A., Schewe, B., Neuschäfer-Rube, F., Ringel, S., Neuber, C., Kleuser, B., Püschel, G.P., 2015. Enhanced thyroid hormone breakdown in hepatocytes by mutual induction of the constitutive androstane receptor (CAR, NR1I3) and arylhydrocarbon receptor by benzo[a]pyrene and phenobarbital. Toxicology 328, 21–28.
Seemann, F., Peterson, D.R., Witten, P.E., Guo, B.S., Shanthanagouda, A.H., Ye, R.R., Zhang, G., Au, D.W.T., 2015. Insight into the transgenerational effect of benzo[a] pyrene on bone formation in a teleost fish (Oryzias latipes). Comp. Biochem. Physiol. Part - C. Toxicol. Pharm. 178, 60–67.
Seemann, F., Jeong, C.B., Zhang, G., Wan, M.T., Guo, B., Peterson, D.R., Lee, J.S., Au, D. W., 2017. Ancestral benzo[a]pyrene exposure affects bone integrity in F3 adult fish (Oryzias latipes). Aquat. Toxicol. 183, 127–134.
Shi, Q., Godschalk, R.W.L., van Schooten, F.J., 2017. Inflammation and the chemical carcinogen benzo[a]pyrene: partners in crime. Mutat. Res. Rev. Mutat. Res. 774, 12–24.
Shin, K.H., Kim, K.W., Ahn, Y., 2006. Use of biosurfactant to remediate phenanthrene-contaminated soil by the combined solubilization-biodegradation process. J. Hazard. Mater. 137 (3), 1831–1837.
Singh, S.P., Holdway, J.E., Poss, K.D., 2012. Regeneration of amputated zebrafish fin rays from *de novo* osteoblasts. Dev. Cell 22 (4), 879–886.
Sinha, K.M., Zhou, X., 2013. Genetic and molecular control of osterix in skeletal formation. J. Cell. Biochem. 114 (5), 975–984.
Song, J.Y., Casanova-Nakayama, A., Möller, A.M., Kitamura, S.I., Nakayama, K., Segner, H., 2020. Aryl hydrocarbon receptor signaling is functional in immune cells of rainbow trout (Oncorhynchus mykiss). Int. J. Mol. Sci. 21 (17), 1–15.
Stockinger, B., Meglio, P.Di, Gialitakis, M., Duarte, J.H., 2014. The aryl hydrocarbon receptor: multitasking in the immune system. Annu. Rev. Immunol. 32 (1), 403–432.
Sugisaki, R., Miyamoto, Y., Yoshimura, K., Sasa, K., Kaneko, K., Tanaka, M., Itose, M., Inoue, S., Baba, K., Shirota, T., Chikazu, D., Kamijo, R., 2020. Possible involvement of elastase in enhanced osteoclast differentiation by neutrophils through degradation of osteoprotegerin. Bone 132, 115216. October 2019.
Suvarapu, L.N., Baek, S.O., 2017. Review on the concentrations of benzo[a]pyrene in the Indian Environment Since 1983. Polycycl. Aromat. Compd. 37 (4), 235–256.
Suzuki, N., Sato, M., Nassar, H.F., Abdel-Gawad, F., Bassem, S.M., Yachiguchi, K., Tabuchi, Y., Endo, M., Sekiguchi, T., Urata, M., Hattori, A., Mishima, H., Shimasaki, Y., Oshima, Y., Hong, C.S., Makino, F., Tang, N., Toriba, A., Hayakawa, K., 2016. Seawater polluted with highly concentrated polycyclic aromatic hydrocarbons suppresses osteoblastic activity in the scales of Goldfish, Carassius auratus. Zool. Sci. 33 (4), 407–413.
Tang, R., Dodd, A., Lai, D., McNabb, W.C., Love, D.R., 2007. Validation of zebrafish (Danio rerio) reference genes for quantitative real-time RT-PCR normalization. Acta Biochim. Biophys. Sin. 39 (5), 384–390.
Tarasco, M., Laizé, V., Cardeira, J., Cancela, M.L., Gavaia, P.J., 2017. The zebrafish operculum: a powerful system to assess osteogenic bioactivities of molecules with pharmacological and toxicological relevance. Comp. Biochem. Physiol. Part C. Toxicol. Pharm. 197, 45–52.
Tarasco, M., Cordelières, F.P., Cancela, M.L., Laizé, V., 2020. ZFBONE: an ImageJ toolset for semi-automatic analysis of zebrafish bone structures. Bone 138, 115480.
Torvanger, I., Metz, J.R., Olsvik, P.A., Søfteland, L., Lie, K.K., 2018. Benzo(a)pyrene reduces osteoclast and osteoblast activity in ex-vivo scales of zebrafish (Danio rerio [Hamilton-Buchanan, 1822]) and goldfish (Carassius auratus [Linnaeus, 1758]). J. Appl. Ichthyol. 34 (2), 431–439.
van de Peppel, J., Franceschi, R.T., Li, Y., van der Eerden, B.C.J., 2018. Vitamin D regulation of osteoblast function. Vitamin D, fourth ed. Elsevier, pp. 295–308.
Vimalraj, S., 2020. Alkaline phosphatase: structure, expression and its function in bone mineralization. Gene 754, 144855.
de Vrieze, E., van Kessel, M.A.H.J., Peters, H.M., Spanings, F.A.T., Flik, G., Metz, J.R., 2014. Prednisolone induces osteoporosis-like phenotype in regenerating zebrafish scales. Osteoporos. Int. 25 (2), 567–578.
Walker, M.B., Kimmel, C.B., 2007. A two-color acid-free cartilage and bone stain for zebrafish larvae. Biotech. Histochem. Publ. Biol. Stain Comm. 82 (1), 23–28.
Williams, M.A., Salice, C., Reddy, G., 2015. Wildlife toxicity assessment for benzo[a] pyrene. Wildlife Toxicity Assessments for Chemicals of Military Concern. Elsevier, pp. 421–437.
Witten, P.E., 1997. Enzyme histochemical characteristics of osteoblasts and mononucleated osteoclasts in a teleost fish with acellular bone (Oreochromis niloticus, Cichlidae). Cell Tissue Res. 287 (3), 591–599.
Witten, P.E., Hall, B.K., 2015. Teleost skeletal plasticity: modulation, adaptation, and remodelling. Copeia 103 (4), 727–739.
Wright, H.L., Moots, R.J., Bucknall, R.C., Edwards, S.W., 2010. Neutrophil function in inflammation and inflammatory diseases. Rheumatology 49 (9), 1618–1631.
Xie, S., Zhou, A., Xu, N., Feng, Y., Pan, Z., Junaid, M., Wang, J., Zou, J., 2020. Benzo[a] pyrene induces microbiome dysbiosis and inflammation in the intestinal tracts of western mosquitofish (Gambusia affinis) and zebrafish (Danio rerio). Fish. Shellfish Immunol. 105, 24–34.
Yang, S.C., Tsai, Y.F., Pan, Y.L., Hwang, T.L., 2020. Understanding the role of neutrophils in acute respiratory distress syndrome. Biomed. J. 1–8.
Yu, H., Jiang, L., Wan, B., Zhang, W., Yao, L., Che, T., Gan, C., Su, N., He, J., Huang, J., Zhang, K., Zhang, Y., 2018. The role of aryl hydrocarbon receptor in bone remodeling. Prog. Biophys. Mol. Biol. 134 (1), 44–49.
Zarei, A., Morovat, A., Javaid, K., Brown, C.P., 2016. Vitamin D receptor expression in human bone tissue and dose-dependent activation in resorbing osteoclasts. Bone Res. 4 (1), 1–10.
Zhang, S., Yao, H., Lu, Y., Yu, X., Wang, J., Sun, S., Liu, M., Li, D., Li, Y.F., Zhang, D., 2017. Uptake and translocation of polycyclic aromatic hydrocarbons (PAHs) and heavy metals by maize from soil irrigated with wastewater. Sci. Rep. 7 (1), 1–11.
Zhou, J., Maskaoui, K., 2003. Distribution of polycyclic aromatic hydrocarbons in water and surface sediments from Daya Bay, China. Environ. Pollut. 121 (2), 269–281.
Zhou, Y., Jiang, R., An, L., Wang, H., Cheng, S., Qiong, S., Weng, Y., 2017. Benzo[a] pyrene impedes self-renewal and differentiation of mesenchymal stem cells and influences fracture healing. Sci. Total Environ. 587–588, 305–315.
Zodrow, J.M., Tanguay, R.L., 2003. 2,3,7,8-tetrachlorodibenzo-P-dioxin inhibits zebrafish caudal fin regeneration. Toxicol. Sci. 76 (1), 151–161.
Lawal, AT., 2017. Polycyclic aromatic hydrocarbons. A review. Cogent Environ Sci 3, 1.